Přírodovědecká fakulta
Faculty of Science

Jihočeská univerzita v Českých Budějovicích
University of South Bohemia in České Budějovice

Specimen preparation for Serial-Block Face Scanning Electron Microscopy and Contrast Evaluation by Transmission Electron Microscopy

Bachelor Thesis

submitted by
Dominik Baumann

carried out at
Laboratory of Electron Microscopy, Biology Centre

supervised by
RNDr. Marie Vancová, Ph.D.
and
Mgr. Tomáš Bílý

České Budějovice, 2018

Baumann, D., 2018: Specimen preparation for Serial-Block Face Scanning Electron Microscopy and Contrast Evaluation by Transmission Electron Microscopy. Bc. Thesis, in English. – 39p., Faculty of Science, University of South Bohemia, České Budějovice, Czech Republic.

Annotation

Lanthanide salts were tested as alternative heavy metal stains to uranyl acetate for the sample preparation for serial block-face scanning electron microscopy. The influences of section thickness and the application of microwave radiation during sample preparation on the contrast of sections in transmission electron microscopy were also examined.

Declaration

I hereby declare that I have worked on my bachelor's thesis independently and used only the sources listed in the bibliography. I hereby declare that, in accordance with Article 47b of Act No. 111/1998 in the valid wording, I agree with the publication of my bachelor thesis, in full to be kept in the Faculty of Science archive, in electronic form in publicly accessible part of the STAG database operated by the University of South Bohemia in České Budějovice accessible through its web pages. Further, I agree to the electronic publication of the comments of my supervisor and thesis opponents and the record of the proceedings and results of the thesis defence in accordance with aforementioned Act No. 111/1998. I also agree to the comparison of the text of my thesis with the Theses.cz thesis database operated by the National Registry of University Theses and a plagiarism detection system.

České Budějovice, 14.5.2018

Dominik Baumann

Acknowledgements

Here I would like to express my gratitude towards my supervisors RNDr. Marie Vancová and Mgr. Tomáš Bílý for their guidance, advice and patience. I also would like to thank the other members of the laboratory for electron microscopy for their never-ending support during this project.

Contents

1. Introduction and Goals

1.1 Goals

The goal of this work was to evaluate a replacement stain for Uranyl acetate for the preparation of samples for serial-block face scanning electron microscopy ("SBF-SEM"). The criteria for evaluation were the overall image quality in a scanning electron microscope (which is mainly affected by the sample's conductivity) and image contrast in a transmission electron microscope. The SBF-SEM procedure was not carried out in this work.

1.2 Basic principles of electron microscopy

Back in 1823, Ernst Abbe calculated the maximum resolution of light microscopes to be 187 nm. In the 1930s, Louis de Broglie's wave-particle theory sparked the idea to use electrons for imaging applications. De Broglie showed that an electron's wavelength is short enough to reach far greater resolutions than any type of light microscope [1; 2]. In consequence, the essential feature of electron microscopes is that they use electrons instead of light to obtain images at much higher resolution, which makes it possible to study tiniest biological structures such as cell organelles.

In general, electron microscopes are operated in a state of high-vacuum. This prevents unwanted electrical discharge and protects the electrons' trajectory from being influenced by gas or hydrocarbon molecules. Another positive effect of the vacuum is the reduced presence of contaminants that might deposit on the specimen. A nitrogen-cooled copper rod inside the vacuum chamber is used to attract contaminants, improving the vacuum [2; 3].

The most common source of electrons in electron microscopes is a filament, a tungsten wire that is surrounded by a cathode cap. The accelerating voltage is applied to the cathode cap and a small potential difference between the cap and the filament is caused by a resistor. Below this electron gun, an anode is located, which attracts and accelerates the electrons from the filament (Figure 1). The trajectory of the emitted electrons is then controlled by an assembly of circularly shaped, electromagnetic lenses and metal apertures (Figure 1) [2; 3].

The main purpose of the lenses is to correctly focus on and illuminate the specimen, while also providing proper magnification. Only as little area of the specimen as necessary should be exposed to the electron beam in order to reduce damage caused by the electron beam [2–4].

The electron micrograph is recorded with a CCD camera. The formation of the image is a result of the electrons' interactions with heavy metals that have been introduced to the sample.

The origin of the signal that the CCD camera records depends on the type of electron microscope and is described in the following sections.

Just as light microscopes, electron microscopes might suffer from spherical or chromatic aberrations, negative effects on the image quality that can be reduced by the lenses and apertures. Spherical aberration (Figure 2) results from the fact that the lenses direct electrons differently depending on how close to the central axis the electrons pass through the lens opening. Electrons that pass close to the central axis are refracted less than electrons that pass close to the actual magnet. An aperture allows only the electrons close to the central axis to pass the lens. Electrons with different energies lead to chromatic aberration – depending on their energy, electrons are refracted to a different extent by the lens. Chromatic aberration (Figure 2) can be reduced by increasing the accelerating voltage [2; 3].

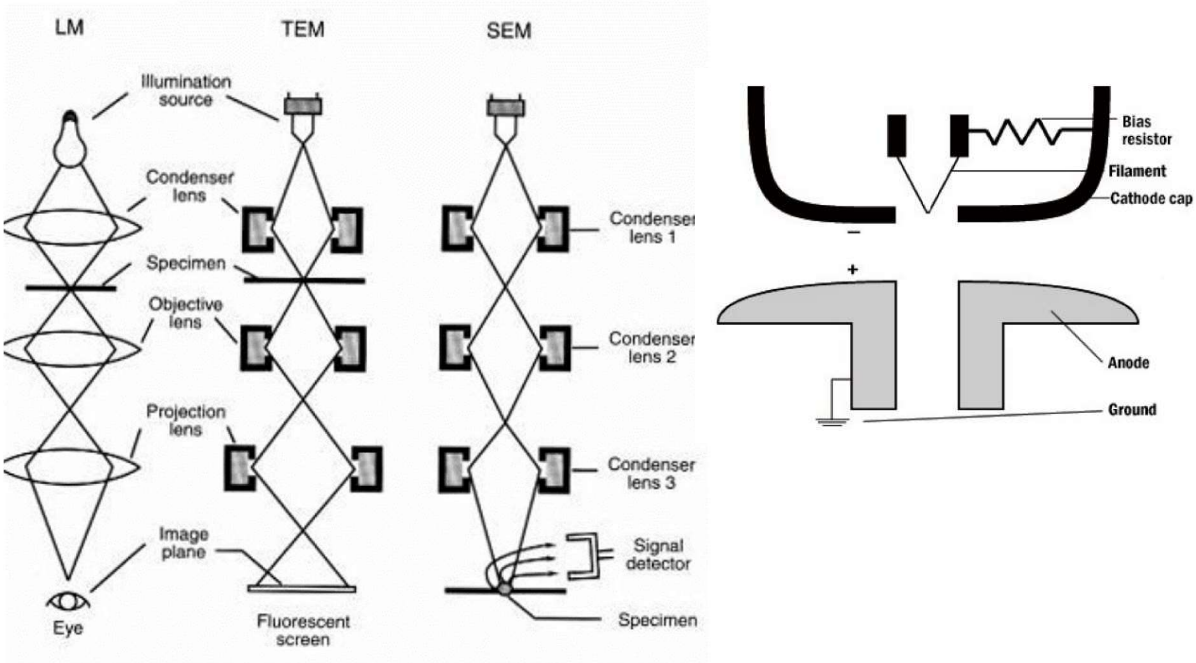

Figure 1: *Left:* Comparison of the basic setups of a light microscope (LM), a TEM and an SEM; *Top right:* Layout of an electron gun. Images taken form [2]

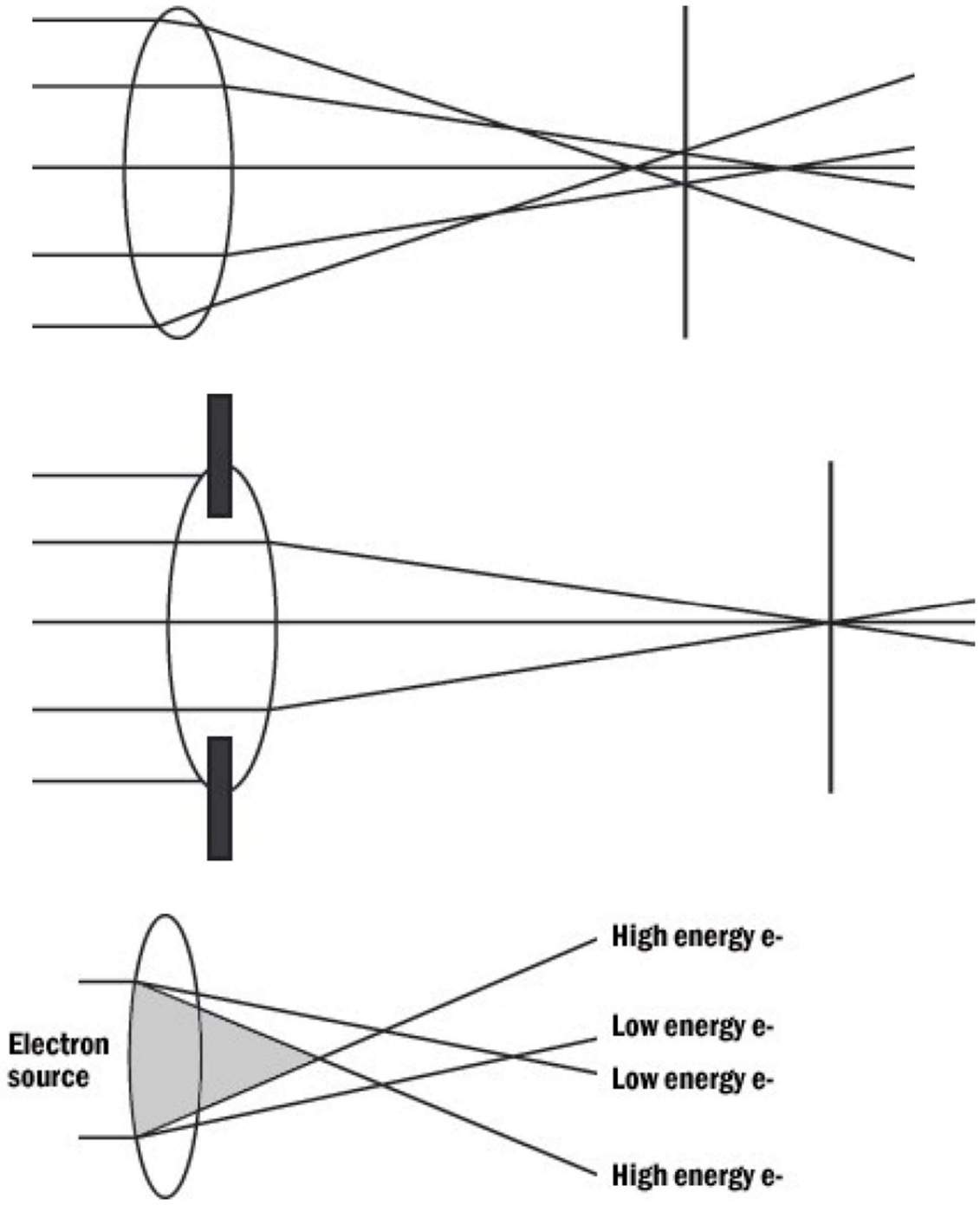

Figure 2: *Top:* Illustration of spherical aberration; *Middle:* Reduction of spherical aberration by using an aperture; *Bottom:* chromatic aberration of electrons with different energies; Images taken from [2]

A few more explanations:

The observed specimen might appear to move across the screen. This phenomenon is known as drift and is caused by either contaminants in the vacuum or the build-up of heat and static charges [2].

The dose is the number of electrons hitting the sample per unit area. The higher the dose, the more the sample is destroyed by the electron beam [5].

Together with the apertures, the accelerating voltage is the main parameter that specifies the resolution. Two points that are close by are properly resolved, when they can be identified as separate entities. A high accelerating voltage and a small aperture increase resolution [2; 3].

1.3 Transmission electron microscopy

As previously mentioned, the electrons' interactions with heavy metals in the sample give rise to image formation. Due to these interactions the beam electrons may change their direction either without energy losses (elastic scattering) or with energy losses (inelastic scattering). In the case of TEM working at 100-200 kV, the sample is a thin layer (e.g. an ultrathin section, ca. 70 nm thick, cut from a larger piece of biological tissue). In order to obtain images, the sample has to be stained with heavy metals – the staining procedure is described in more detail in one of the following sections. Due to their higher atomic number, heavy metals increase the elastic scattering of electrons – similarly, thicker specimens also increase the elastic scattering of electrons [6]. The electron micrograph is then obtained from the observed scattering pattern. In order to reduce the destructive effect of the electron beam on the sample, a layer of carbon can be sputtered on the sections [2; 4].

The scattering of electrons can either be elastic or inelastic. Elastic scattering changes the trajectory of the electrons, but not their energy. On the other hand, during an inelastic scattering process energy is transferred between electrons and the atoms they impact on [2; 3].

1.4 Scanning electron microscopy

In general, the SEM is a versatile instrument used in material science and for the visualization of topography and composition of bulk biological specimen (e.g. entire insects.) Several SEM techniques can be used for the examination of resin-embedded tissue, or sections cut from resin-embedded tissue. In contrast to TEM, the image information is not a result of electrons passing through ("transmit") the sample, but from electrons that are deflected or ejected from the sample [3].

With an SEM, different types of electrons can be detected: Backscattered electrons ("BSE") have been deflected (scattered elastically) away from the specimen's surface. They give images similar to those obtained with TEM, revealing structural information from the layers below the surface [1; 3]. When energy transfers between electrons and specimen atoms occur, several signals can be detected: secondary electrons ("SE"), Auger electrons and characteristic x-rays. Secondary electrons are electrons that are emitted from atoms due to the impact of beam electrons. They can be used to obtain structural information about the surface of the specimen. Auger electrons and the measurement of x-ray energies can be used to investigate the elemental composition of the specimen [3]. Figure 3 illustrates the spatial origin of the various signals in SEM.

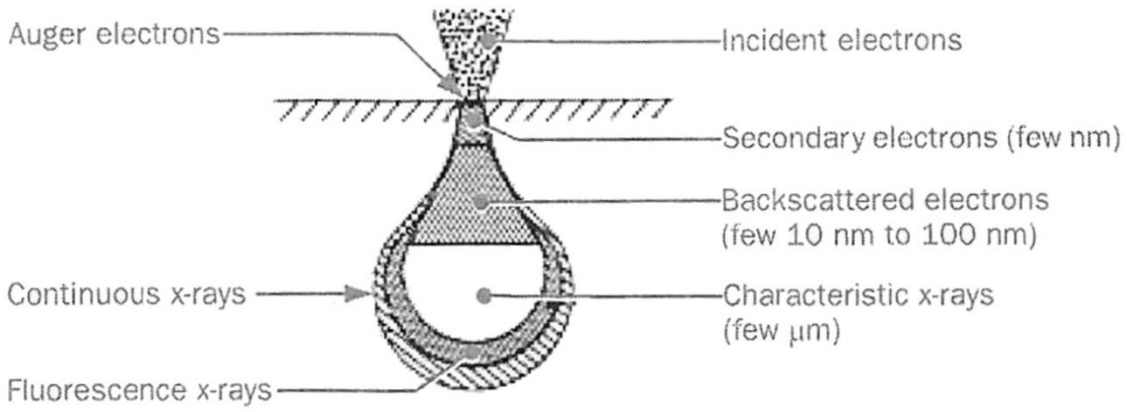

Figure 3: Origin of signals in SEM; the illustration is taken from JEOL's manual for JSM-7401F

Figure 4 displays the energy levels of the electron signals in SEM: The energy of secondary electrons is much lower than the energy of backscattered electrons. In consequence, secondary electrons can easily be directed towards a positively biased detector. A BSE detector has to cover a larger area, since BSE cannot be artificially directed towards the detector [3]. The principal setup of the SE and BSE detectors is shown in figure 5.

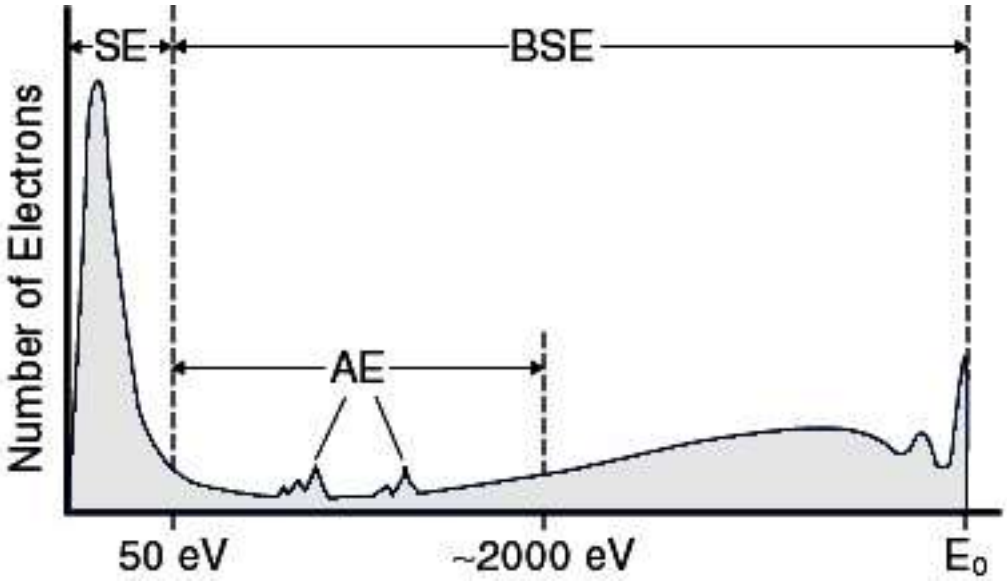

Figure 4: The energy levels of electrons in SEM: secondary electrons ("SE"), backscattered electrons ("BSE") and Auger electrons ("AE"); E_0 is the accelerating voltage/potential; Image taken from [7]

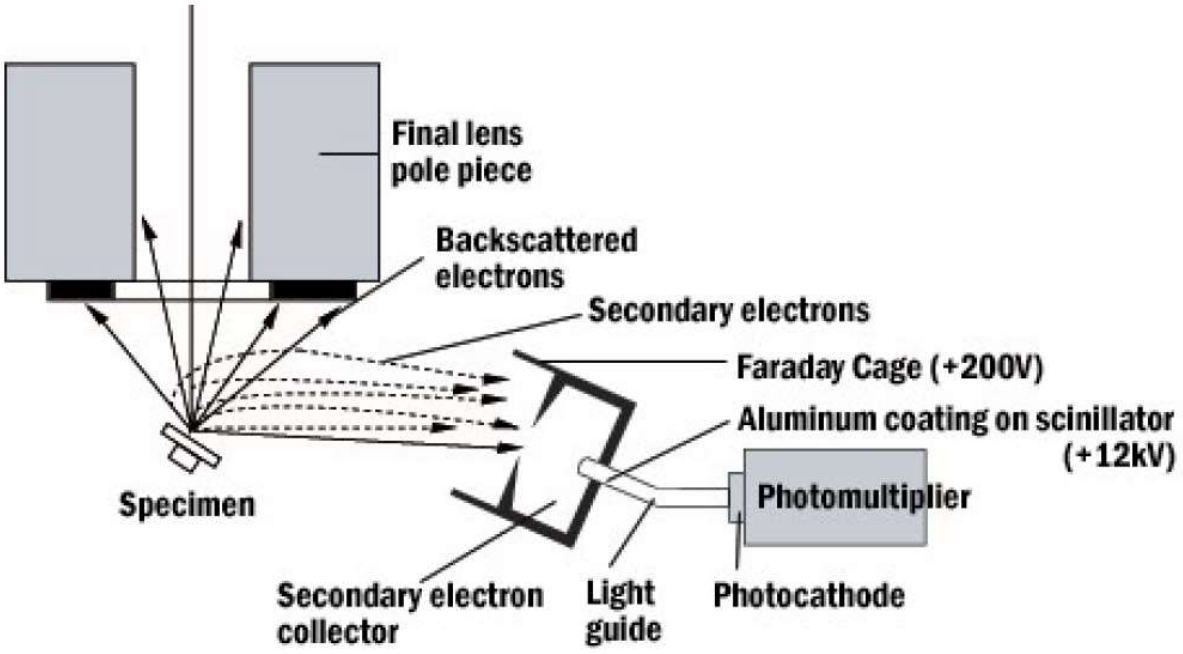

Figure 5: An illustration of the general setup of BSE and SE detectors; Image taken from [3]

The major problem of analysing tissue samples with SEM techniques is charging, which negatively influences the resolution of structures and overall image quality [8]: The tissue samples have to be embedded in non-conductive resin. As a result, the negative charges from the beam accumulate on the specimen surface and cannot be discharged. Thin coats of carbon or metals (e.g. gold, platinum) can be sputtered onto the specimen to provide a conductive layer that prevents accumulation of charges. An alternative to sputter coating has been proposed by a group around Deerinck: precise injection of nitrogen gas over the specimen surface can be used to reduce the effects of charging, while maintaining a high vacuum [3; 8].

A highly interesting application of SEM is the possibility for three-dimensional volume reconstruction of specimens at the nanoscale (x,y-resolution). Compared to light microscopes, electron microscopes offer limited resolution in the z-direction in the BSE mode. The spatial resolution of the BSE is related to the probe size of the beam of primary electrons and is generally larger than its diameter. The BSE volume can be reduced by lowering the accelerating voltage. Several methods involving SEM have been conceived to reconstruct the 3D-structure of specimens [5; 1]. The three most important methods shall be discussed here: Serial Block-Face Scanning Electron Microscopy ("SBF-SEM"), Focused Ion Beam Scanning Electron Microscopy ("FIB-SEM") and Automated Tape-Collecting Ultramicrotome Scanning Electron Microscopy ("ATUM-SEM").

1.4.1 SBF-SEM

SBF-SEM was developed from a concept known as serial section Transmission Electron Microscopy ("ssTEM"): Electron microscopists would cut sections from the sample, image them with TEM and align them manually – a tedious and error-prone task. This method became the blueprint for SBF-SEM. An ultramicrotome was installed inside the sample chamber of an SEM, making it possible to scan the specimen's surface, which was then removed by the ultramicrotome. Repeating this process over and over again results in a set of electron micrographs that can easily be stacked by appropriate software. The advantages of SBF-SEM over ssTEM are obvious: more than significant time saving, easy and automatable image alignment and thus 3D-reconstruction, omission of human error during sectioning, handling and compression/distortion of sections [5]. The concept of SBF-SEM is illustrated in figure 6.

However, SBF-SEM has one major drawback – it is, unlike ssTEM or ATUM-SEM, a destructive method: in ssTEM the sample is cut before it is imaged and can thus be reimaged or further modified. In SBF-SEM, the portion of the specimen that has been imaged is cut off and thus lost to further investigation [5].

Another problem with SBF-SEM is the accumulation of debris from the cut off sections on the specimen. Thus, it is advantageous to briefly inspect the region of interest at low resolution before imaging it at full resolution. If debris is found on the sample, it can be removed with the ultramicrotome's knife [5].

In contrast to FIB-SEM, the voxels in SBF-SEM are originally not isotropic. However, this issue can easily be overcome by varying the accelerating voltage, in order to retrieve information from different depths of the sample [5].

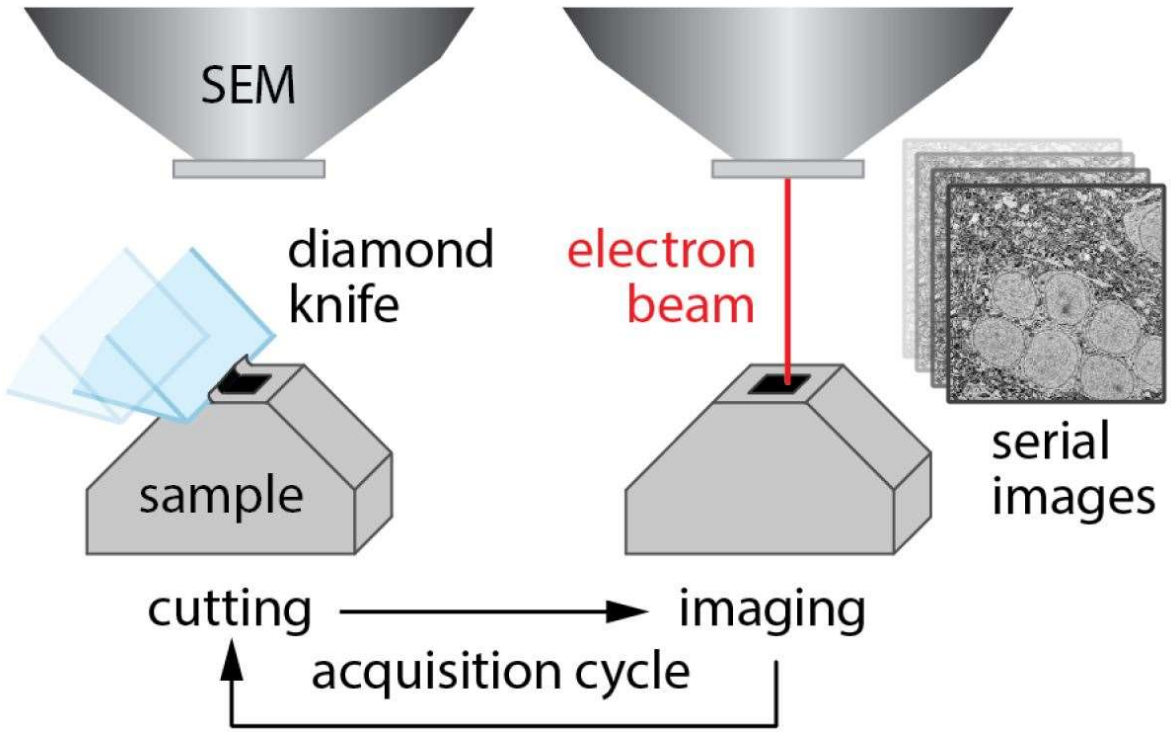

Figure 6: Illustration of the concept of SBF-SEM. The surface of a block is repeatedly imaged and cut off, giving a stack of micrographs that can be used for 3D volume reconstruction of the sample; Image taken from [5]

1.4.2 FIB-SEM

FIB-SEM is similar to SBF-SEM in that it is an iterative process: The specimen surface is imaged and removed repeatedly. The main difference between the two methods is the manner, in which the specimen surface is removed. FIB-SEM makes use of a beam of gallium ions to mill off the specimen surface. Due to the high precision of this technique, surfaces as thin as a few nanometres can be removed during each iteration [5; 1].

This method restricts the size of the specimen surface to approximately 20 micrometres edge length. Otherwise, the ion beam becomes too unfocused to accurately and evenly mill off the specimen surface, resulting in deposits of vaporized materials that negatively affect image quality [5].

As previously mentioned, FIB-SEM like SBF-SEM is a destructive method, which does not allow further processing of the specimen after imaging. On the other hand, the amount of required manual labour is low and the precision of the ion beam makes it easily possible to obtain isotropic voxels (Figure 7) [5].

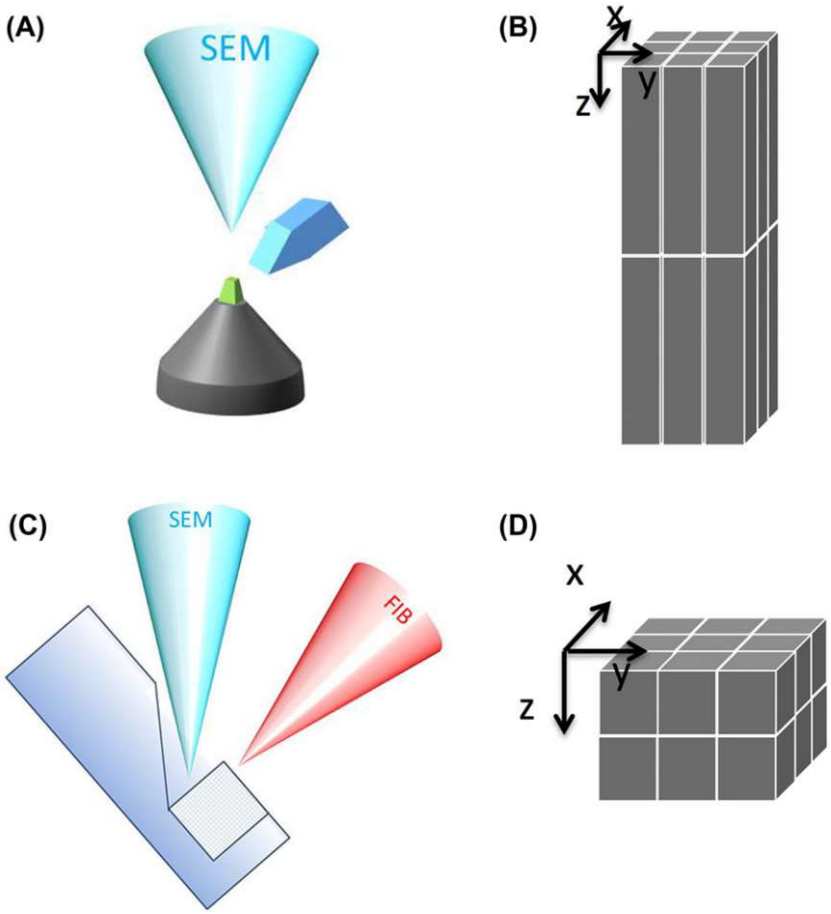

Figure 7: Illustration of non-isotropic voxels obtained in SBF-SEM (A and B) and isotropic voxels obtained in FIB-SEM (C and D); Image taken from [1]

1.4.3 ATUM-SEM

Unlike in FIB-SEM and SBF-SEM, the specimen is cut into ultrathin sections before it is imaged. For this method, the ultramicrotome automatically cuts and collects the ultrathin sections on a tape. Since this tape is not transparent to electrons, the sections cannot be imaged by TEM. Instead the tape is cut into stripes, which are manually mounted on specimen holders for SEM. The sections can then be directly imaged or further modified before that. In consequence, (additional) staining of the sections can be performed after cutting them, whereas samples for SBF-SEM and FIB-SEM have to be stained *en-bloc* [5].

1.5 Aspects of sample preparation

1.5.1 Basic sample preparation

The first step in the preparation of biological samples is chemical fixation, which stops most biological activities in the cells and immobilizes the cell structures. This immobilization is achieved by treating the sample with a solution of glutaraldehyde (and formaldehyde, which is prepared by depolymerization of paraformaldehyde). The aldehyde groups react with proteins and crosslink them, bringing the processes in the cells to a halt [9; 10]. The reaction schemes of formaldehyde and glutaraldehyde with amino groups are displayed in figures 8 and 9.

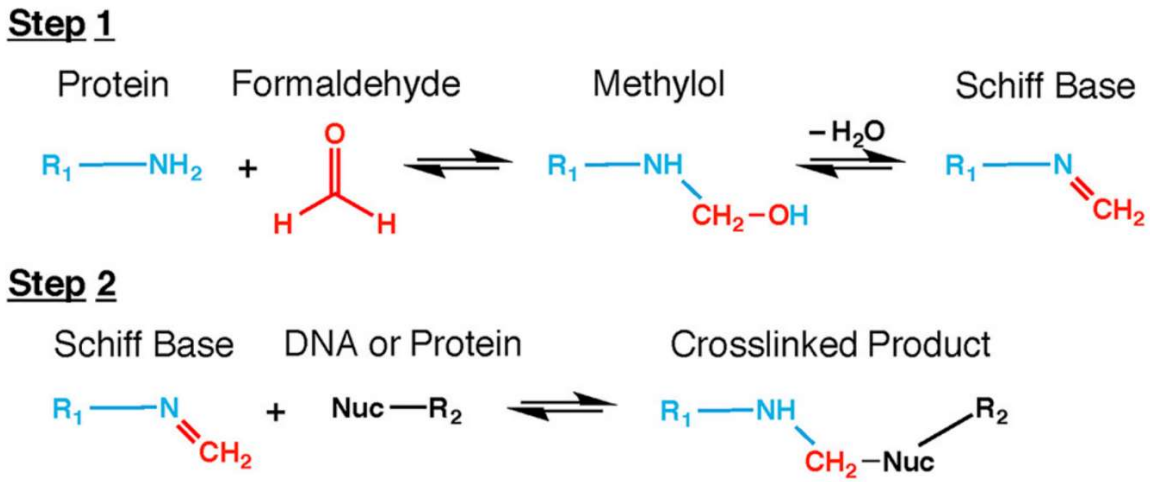

Figure 8: Schematic crosslinking reaction of formaldehyde between an amino-group and another nucleophilic group (e.g. an amino group); Scheme taken from [10]

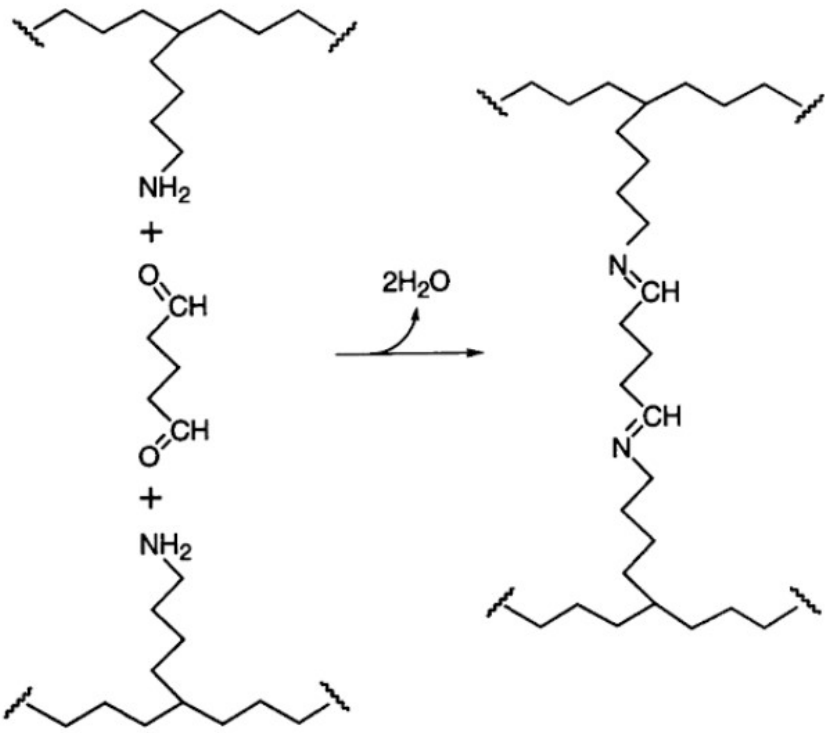

Figure 9: Schematic crosslinking reaction of glutaraldehyde between two amino-groups; Scheme taken from [11]

Secondary fixation ("post-fixation") is carried out with a solution of OsO_4, a process that is much slower than the infiltration with aldehydes. OsO_4 mainly reacts with the double bonds in unsaturated lipids, but can also react slowly with proteins [9]. Switching from it water-soluble form $[OsO_4(OH)_2]^{2-}$ to OsO_4 it can enter the plasma membrane. After entering the plasma membrane, OsO_4 reacts with double bonds in unsaturated lipids, forming cyclic esters as intermediate before dihydroxylation. Following the dihydroxylation step, Osmium is present in the water-soluble form $[OsO_2(OH)_2]^{2-}$, which disproportionates from oxidation state VI into OsO_2 (II) and $OsO_4/[OsO_4(OH)_2]^{2-}$ (VIII). The water insoluble OsO_2 deposits in the lipophilic membrane, causing heavy metal staining, whereas $[OsO_4(OH)_2]^{2-}$ can again react with a double bond. Treating the infiltrated membranes with $K_4[Fe(CN)_6]$ results in improved staining of the membranes: The reducing agent $K_4[Fe(CN)_6]$ reduces $[OsO_4(OH)_2]^{2-}$ to $[OsO_2(OH)_2]^{2-}$, which can then disproportionate, causing additional OsO_2 deposits in the membrane [12]. Treating the samples with TCH before OsO_4 incubation can be used to further increase the deposition of Osmium in the membranes [13].

After treatment with OsO_4, the cells harden significantly, becoming brittle and susceptible to damage. In order to protect the sample material during fixation, it is immersed in a buffer (e.g. phosphate or cacodylate). Cacodylate buffers are preferable, because the phosphate buffers can damage mitochondria [9]. In the previously described fixation step, it is essential to completely depolymerize the paraformaldehyde into formaldehyde, otherwise short-chain formaldehyde oligomers will form a precipitate with the osmium stains, which is non-transparent to the electron beam [9].

Post-fixation with OsO_4 results in the complete permeability of the plasma membranes. In consequence, the osmolality (concentration of osmotically active particles) after post-fixation becomes irrelevant. Using buffers of improper osmolality during primary fixation can significantly affect the cell volume, leading to volume artefacts [14].

Further treatment with other heavy metals can be used to further increase the specimens' contrast as direct consequence of heavy metal deposition in the cells' structures. The most commonly used heavy metals are uranium in the form of uranyl acetate ("UAc") and lead in the form of lead citrate or lead aspartate ("PbAsp"). Applying lead stains after uranium stains has proven to be especially effective, because the uranium stains act as mordant for lead stains, further increasing the achieved contrast [13]. The good staining properties of UAc are assumed to be the result of uranyl ions (UO_2^{2+}) binding to phosphate, carboxylate and sulphide moieties in the sample [15].

Following staining, the samples have to be dehydrated with an ethanol or acetone series before they can be embedded in an epoxy resin. Heating the resin will polymerize it, rendering the samples accessible in hardened polymer blocks, which can easily be stored and processed further.

1.5.2 *En-bloc* staining and microwave-assisted sample preparation

During the preparation of larger tissue samples (such as the mouse brain tissue in this work) for TEM, two different approaches towards post-staining can be taken. The first approach is to post-stain the sample with e.g. UAc and PbAsp directly after fixation and primary staining with aldehydes and OsO_4. The sample is then dehydrated and processed into polymer blocks. This approach is known as *en-bloc* staining.

The second approach is to dehydrate and embed the sample right after fixation and primary staining with aldehydes and OsO_4. Post-staining is then performed after the (ultra)thin sections have been cut from the block. When using lead stains, the procedure should be carried out in a CO_2-free atmosphere and using carbonate-free water to prevent formation of lead carbonate, a precipitate that is non-transparent to the electron beam. Similarly, improper filtering of UAc solutions may lead to precipitation of UAc on the sample [9; 13].

The general advantage of *en-bloc* staining is that it is more convenient: Several tissue entities can be stained simultaneously, whereas otherwise the (ultra)thin sections have to be stained separately. However, care has to be taken to avoid poor contrast of *en-bloc* stained specimens as a result of insufficient or uneven stain penetration [13]. Some studies suggest that the use of microwave radiation can significantly speed up the (*en-bloc*) preparation process and improve the results of fixation while showing no detrimental effects [13; 16].

1.5.3 Replacement stains

A serious drawback of uranium- and lead-based stains is their handling – aside from uranium being radioactive, they are also extremely toxic. In order to reduce problems and cost with the disposal of these stains, and also to reduce the hazard potential for the lab workers, alternative stains are constantly being searched for and tested. Such replacement stains include platinum blue, hafnium chloride and meglumine gadoterate. However, these stains tend to be less stable in aqueous solution and also provide less contrast than UAc. On the other hand, promising results have been achieved with the use of samarium triacetate (“SmAc”), gadolinium triacetate (“GdAc”), ytterbium triacetate (“YbAc”) and lutetium triacetate (“LuAc”), with these stains giving contrast comparable to UAc [15].

2. Results and Discussion

2.1 Primary sample preparation

The staining of the samples was successful for all batches. Specimen from batches T46a/b/c were examined preliminarily by TEM and showed preserved cell structures. Heavy metal deposits were absent, and the penetration of heavy metals appeared to be even. Specimen from batches T43a/b/c were not examined before image acquisition for contrast evaluation. Transmission electron micrographs of the preliminary examination of T46a/b/c are shown in figures 10-12.

Table 1: Overview of the prepared samples, indicating the used stains and the application of microwave radiation during sample preparation

	T43			T46		
	a	b	c	a	b	c
Microwaved	no	no	no	yes	yes	yes
Stain	UAc	GdAc, SmAc	-	UAc	GdAc, SmAc	-

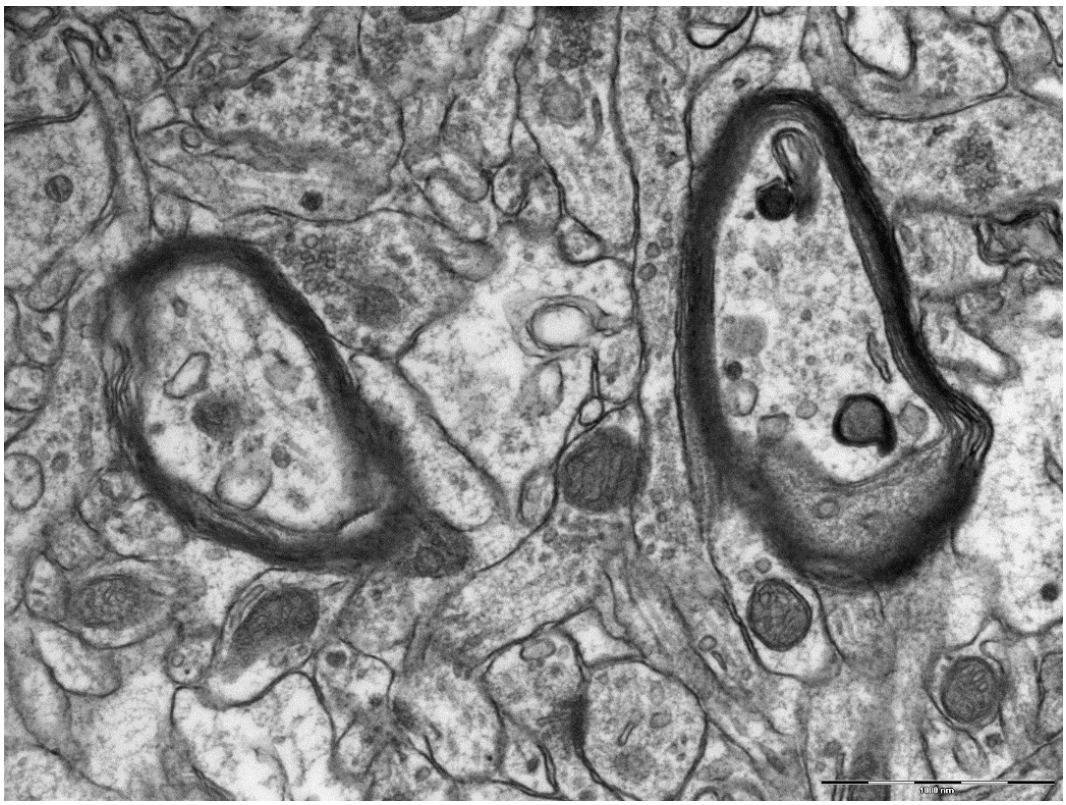

Figure 10: Electron micrograph of T46a; the bar in the lower right edge corresponds to 1 µm

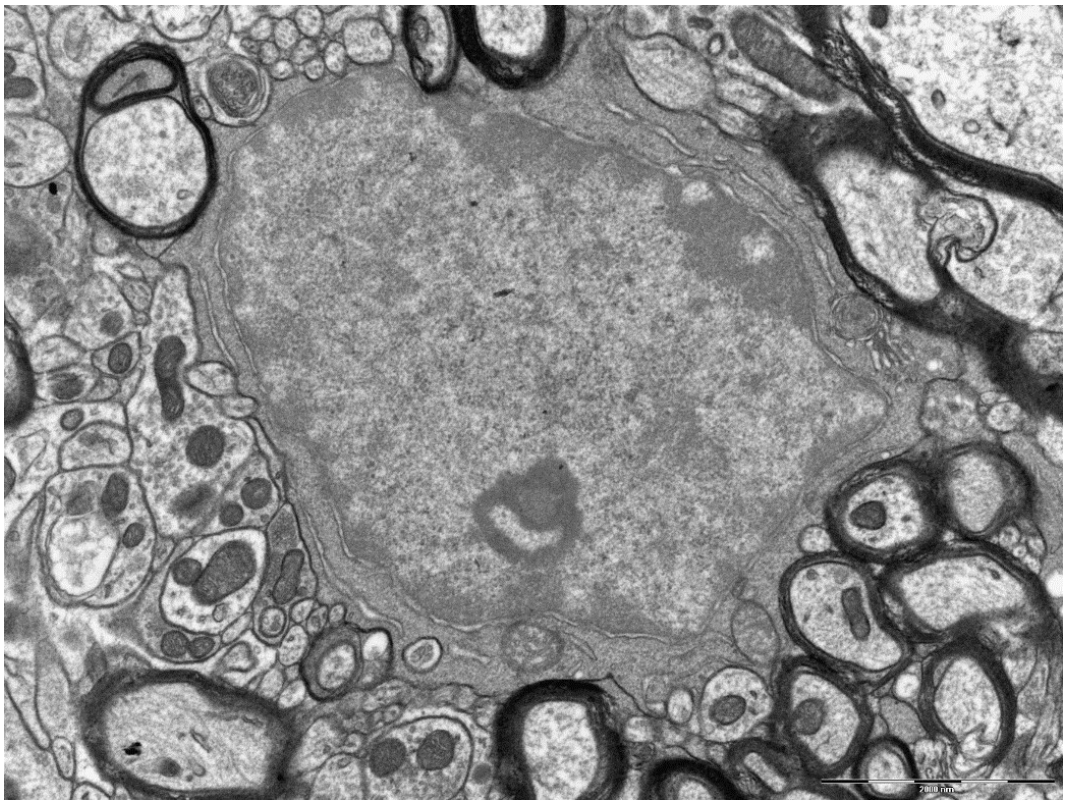

Figure 11: Electron micrograph of T46b; the bar in the lower right edge corresponds to 2 µm

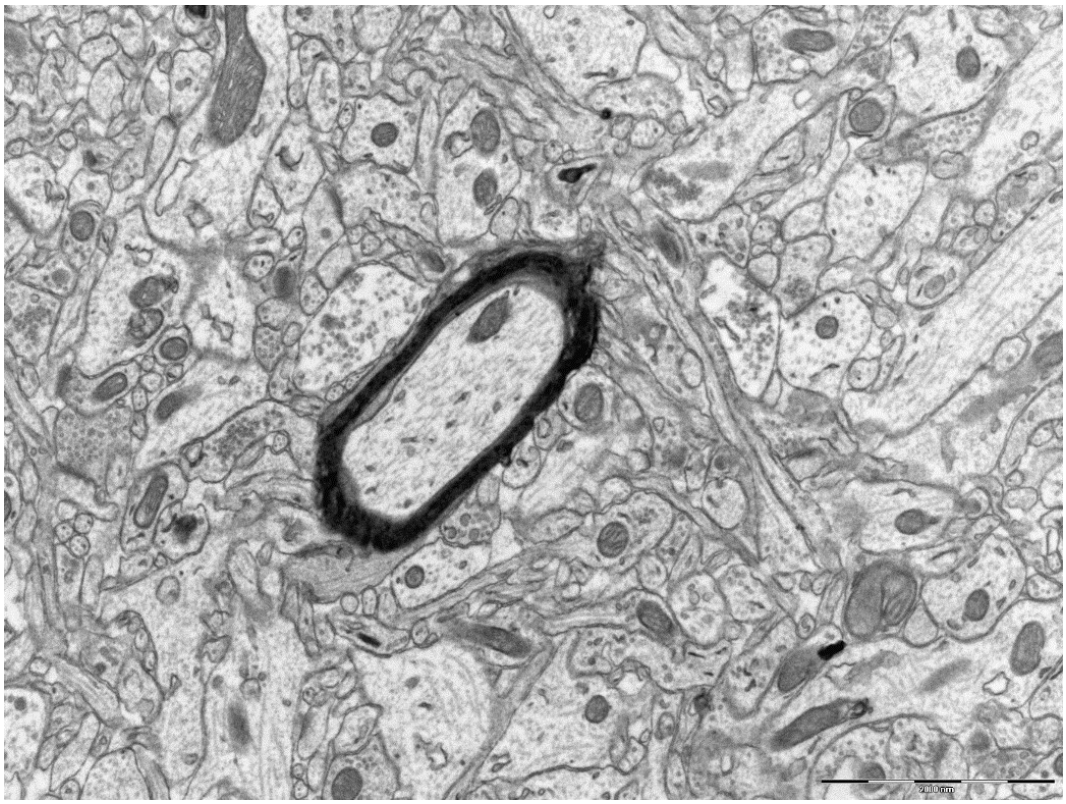

Figure 12: Electron micrograph of T46c; the bar in the lower right edge corresponds to 2 µm

2.2 Examination of charging in SEM

Cubes with 200 nm edge length were prepared from T46a/b/c (one each) for SBF-SEM. The extent of charging for the differently stained batches T46a/b/c was evaluated by SEM.

T46c exhibited much more charging than T46a, which mainly showed charging artefacts at the nuclei. This is not really a surprising result, since T46a was additionally stained with UAc and PbAsp, whereas T46c was only stained with OsO_4 – as a result, T46c contains less metal ions and is thus less conductive as T46a, allowing for more charge accumulation. Nevertheless, the structural features were observable in both cases (in regions that were not charged). Several electron micrographs of T46a and T46c are shown in figure 13.

T46b (Figure 14) exhibited by far the most charging, which rendered the sample worthless for processing by SBF-SEM. The low conductivity of T46b and T46c might have resulted from insufficient grounding to the specimen stage with silver paint or improper sputter coating. However, the examination of two more cubes of T46a and T46b yielded the same result as before: the T46a cubes showed little to no charging, whereas the T46b samples where more or less useless for SBF-SEM. Thus, there has to be a problem with the replacement stain. The charging was also observed in BSE mode (data/micrographs not shown).

It would be interesting to see, if Deerinck's method of focal gas injection [8] would be able to sufficiently reduce the charging of T46b for an investigation by SBF-SEM, and thus enabling the evaluation of contrast in SEM. Recently, another approach to reducing charging has been demonstrated by embedding tissues into resins whose conductivity was increased by adding Ketjen carbon black [17].

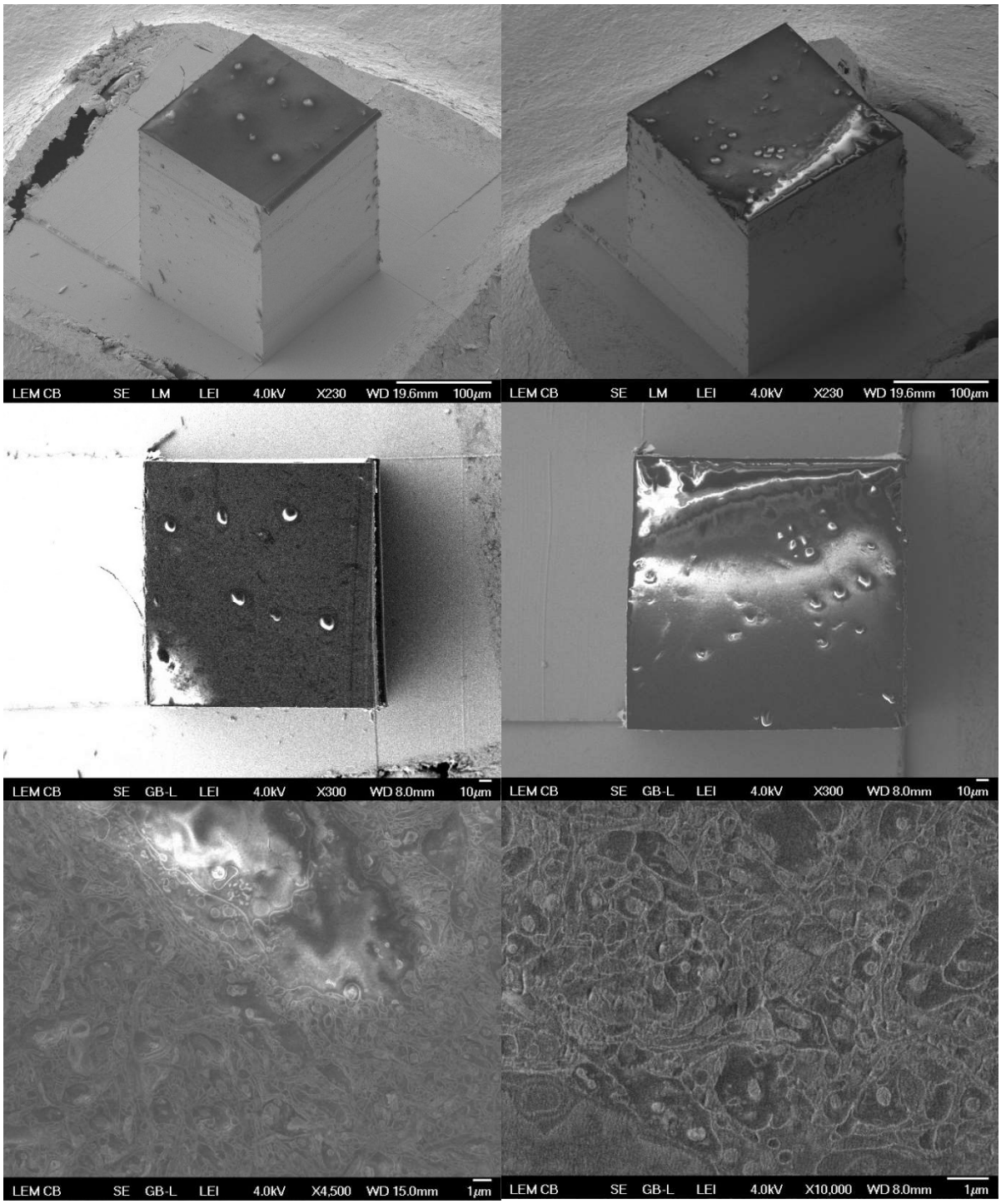

Figure 13: Electron micrographs of T46a (left) and T46c (right); side view (top), top view (middle), detail of the top surface (bottom); all micrographs were acquired with the LEI detector

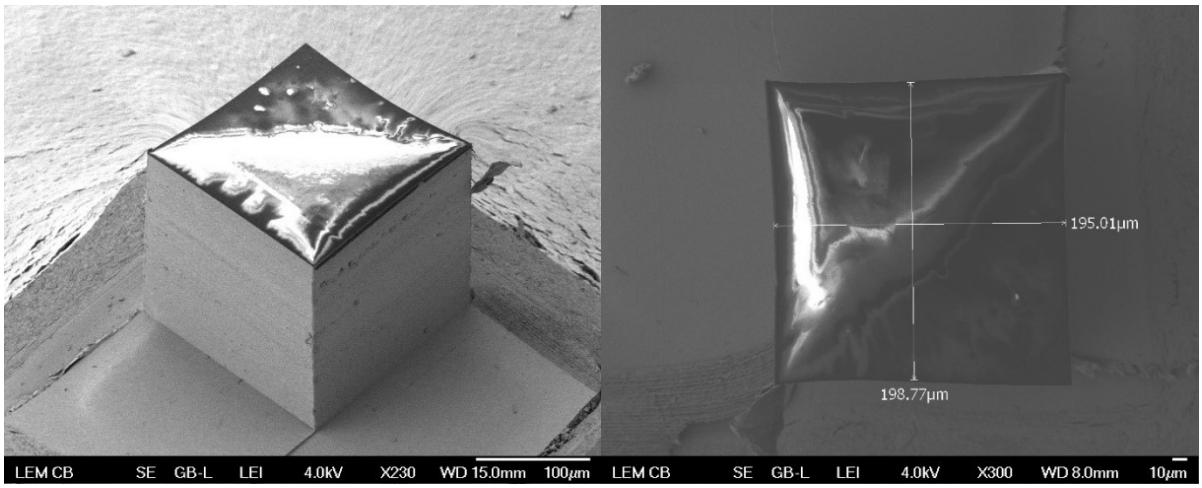

Figure 14: Electron micrographs of T46b; side view (left) and top view with the measured dimensions of the cube (right); both images were acquired with the LEI detector

2.3 Contrast evaluation

The contrast of the samples was evaluated by TEM, using different calculation methods for the contrast (see experimental section). The recorded images of tissue-free resin were not used for the evaluation.

Global contrast:

At first, the mean global contrasts of the entire images were calculated for each group in two different ways (Figures 15 and 16). The problem with global contrast is that it is less an indication of membrane contrast, but rather an overall image statistic. Also, the calculation is influenced by the presence of extreme (very high or low) grey values. The problem of extremes is reduced by including the standard deviation in the second calculation.

The second calculation suggests that the control group (no additional staining) has the highest contrast of all groups. Also, the contrast of thicker sections (90 nm) of T46a was calculated to be (slightly) lower than the contrast of sections with 70 nm thickness. The contrast of T46b was calculated to be lower than that of T46a (70 nm).

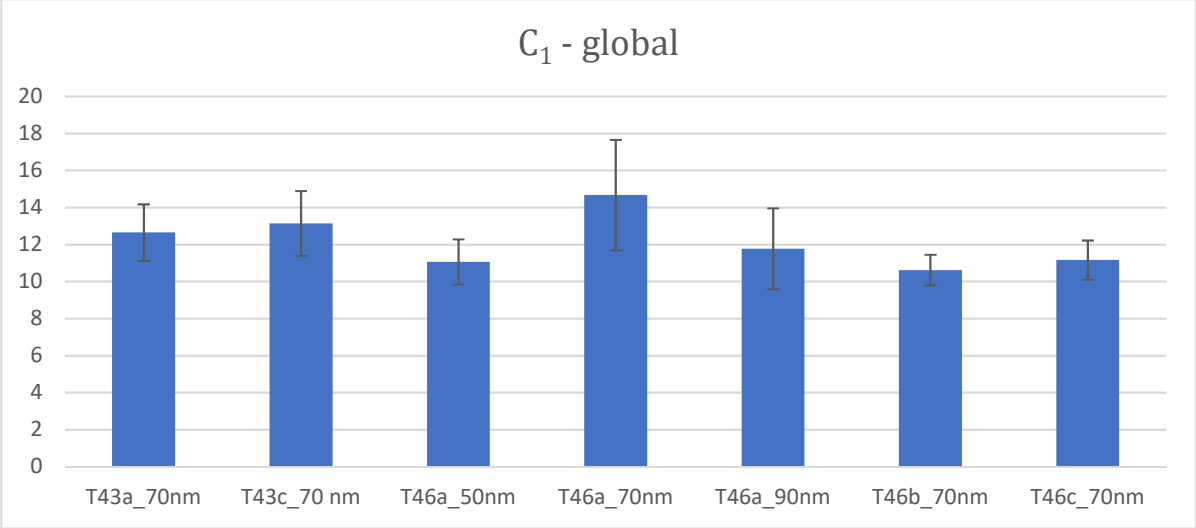

Figure 15: Calculated Michelson contrasts of the different samples; Calculated from whole images without preselection of membranes

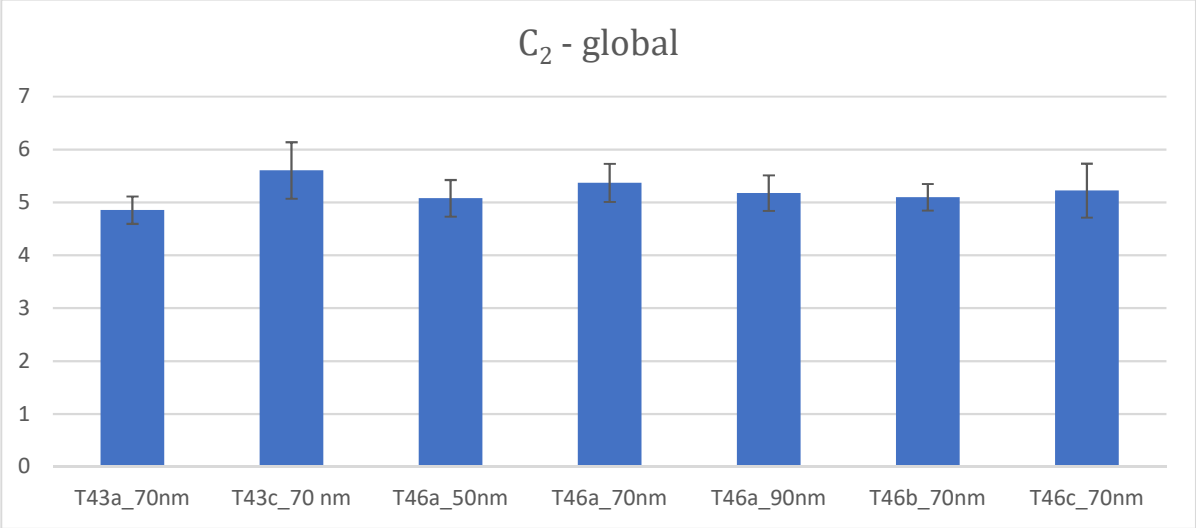

Figure 16: Calculated contrasts of the different samples; Calculated from whole images without preselection of membranes

Automated Measurement of Membrane Contrast:

The Michelson contrast was calculated again (Figure 17), but this time the membranes were automatically preselected by ImageJ. As a consequence, the mean grey values of the membranes and the background could be used as minimum and maximum grey values in the calculation of the Michelson contrast. This procedure should give a better representation of the membrane contrast than the global contrast calculations. The calculation suggested that the contrasts were higher when the samples had not been microwaved (T43a/c and T46a/c). The contrast of T46b was a little bit lower than that of T46a (70 nm), and lower than that of T43a and T43c. In contrast to the global measurements the contrast of T46a sections with 70 nm thickness was lower than that with 90 nm but also than that with 50 nm. Taking into account the standard deviations, the samples that had been stained with UAc (T43a and T46a) would have the highest contrast.

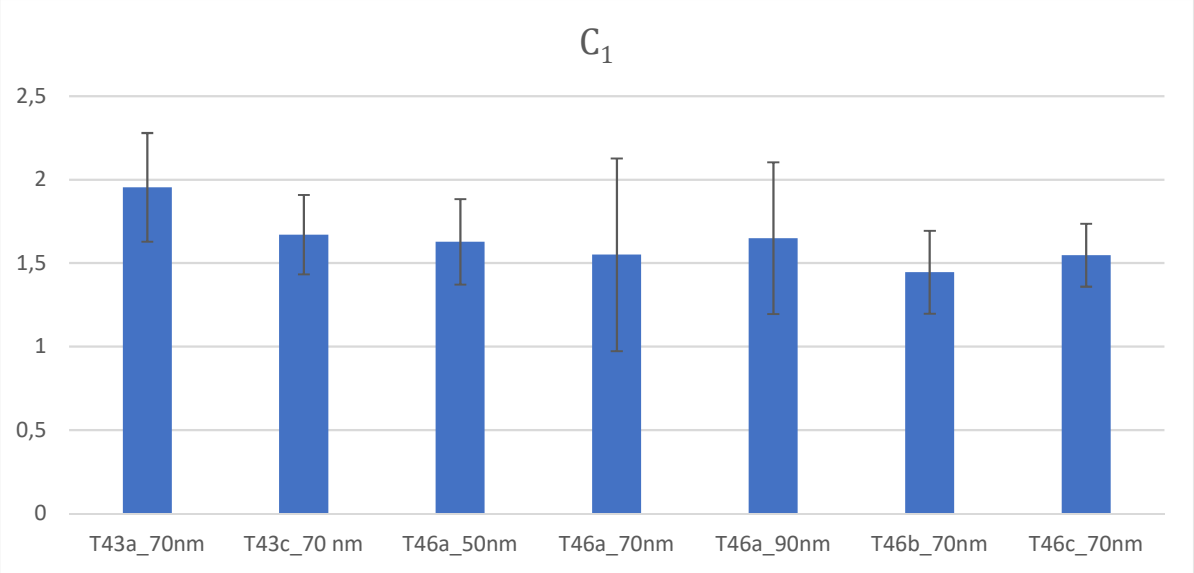

Figure 17: Calculated Michelson contrasts of the different samples; Calculated with automated preselection of membranes by ImageJ

Manual Measurement of Membrane Contrast – Sigmoid Fit:

For this calculation the grey values of the membranes were measured from the centre of the membranes to the background and fitted to a sigmoid function, from which the Michelson contrast was calculated (Figure 18). The calculation suggested that the contrast of T46a (70 nm) was higher than in T43a, T43b and both control groups. Interestingly, the contrast of T46a was again lower at 90 nm than at 70 nm. The contrast of T46b was calculated to be the same as that of T46c.

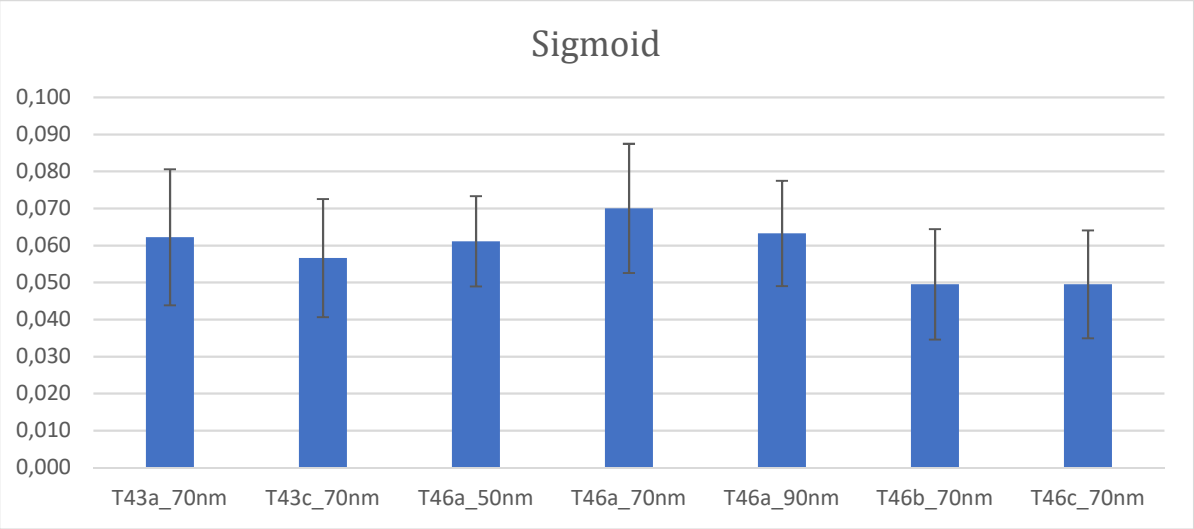

Figure 18: Calculated Michelson contrasts of the different samples; Calculated from manually measured grey values of the membranes

Global Contrast Factor:

The calculation of the Global Contrast Factors ("GCF", Figure 19) suggested that the samples stained with UAc (T43a and T46a) showed the highest contrast. The difference in contrast because of microwaving is relatively small (T43a-T46a, T43c-T46c). The contrast of T46b was smaller than that of T46a. Again, sections of 90 nm thickness showed lower contrast than that with 70 nm thickness.

However, these results are not too meaningful for the contrast of membranes, since the calculation is affected by the amount of structures (cell membranes etc.) in the image – on the other hand, the more images are used for the calculation, the more correct the result, because the amount of structures should level out.

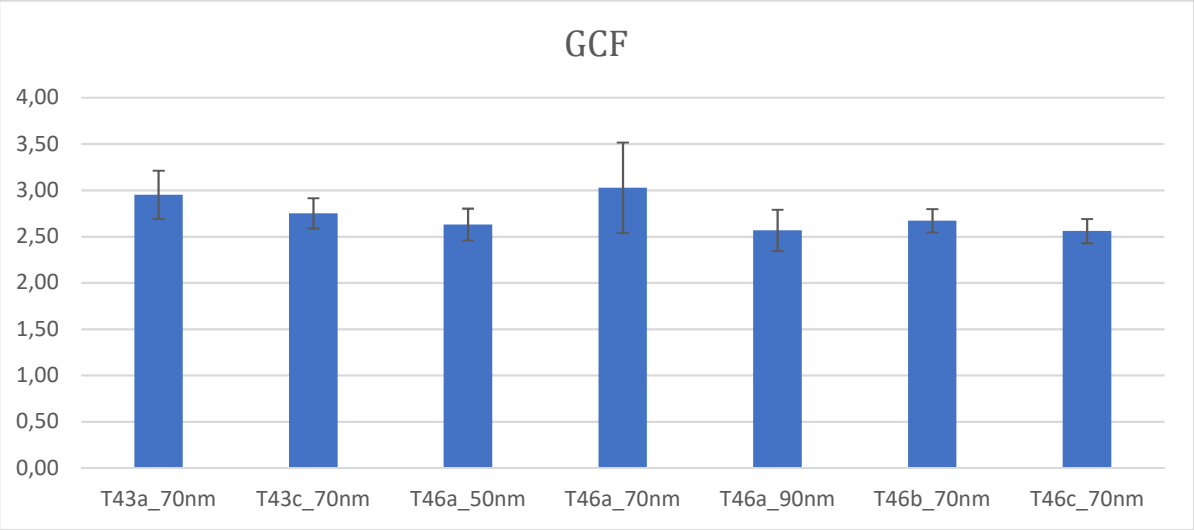

Figure 19: Calculated Global Contrast Factors of the different samples

Conclusions:

Both the Sigmoid and the GCF calculation show that T46a had the highest contrast. Microwaving did not appear to negatively influence the contrast in 70 nm thick sections stained with UAc. Since the contrast of T46b was not measured, no conclusion about the effects of (not) microwaving samples stained with lanthanides can be made.

The application of GdAc and SmAc improved the contrast of the tissue only very slightly. However, the contrast was still sufficient for examining the specimens' ultrastructure. This suggests that the UAc should only be employed for staining, when the highest possible contrast has to be achieved. Otherwise the staining from post-fixation with OsO_4 will be sufficient. Staining with GdAc and SmAc can still be attempted and might give better results for other samples. Other studies have already shown that samarium and gadolinium salts sufficiently stain ultrastructures in samples for TEM and can be used to obtain samples for (SBF-)SEM [1; 18].

Interestingly, the contrast of sections with 90 nm thickness was found to be lower than that of sections with 70 nm thickness (Figure 18). Usually, the contrast increases with the thickness of the section, because more electrons are scattered. It might however be that the sections with 90 nm were already too thick for the used setup, reducing the number of electrons getting through the section and thus decreasing the contrast. It is also possible that the contrast was influenced by the variability of section thickness – the thickness of ultrathin sections is not the same throughout the entire section [19].

For the Sigmoid contrast evaluation, the grey values of plasma membranes of various cell organelles were measured. The measurement and evaluation might be improved by focussing on the plasma membrane of one cell organelle – instead of measuring random membranes, only membranes of e.g. mitochondria could be measured.

Also, a different method for measuring the membrane grey values might be useful: Instead of doing the Sigmoid fit, one could measure the grey values parallel to the membranes and at their centre. If images from tissue-free resin can be shown to have similar grey values as unstained regions of the sample, one could use the mean grey value of the empty resin and the mean grey value of the membranes for the contrast calculation.

All measured grey values can be obtained as supplementary information from the Laboratory of Electron Microscopy, Biology Centre, University of South Bohemia.

The calculated values for the plots in this section can be found in appendix I.

Table 2: Overview of the used methods for contrast calculation

Rank	Method	dependent on structures	dependent on extremes	area
4	Global contrast	independent	dependent	global
2	Automated membrane selection	independent	independent	global/local
1	Sigmoid fit	independent	independent	local
3	GCF	dependent	independent	global

3. Experimental Section

3.1 Sample preparation for SBF-SEM

3.1.1 Chemical fixation and embedding in resin

Tissue samples of 1-2 mm^3 were dissected from the brain of a 6 weeks old, male specimen of Mastomys coucha. The samples were fixed at r.t. for 1 h in 2.5% glutaraldehyde and 2% formaldehyde in a 150 mM sodium cacodylate buffer (pH 7.4), which also contained 2 mM $CaCl_2$. Fixation was continued at 4°C for 15 h. The solution for immersion fixation was freshly prepared by depolymerizing 1 g paraformaldehyde in 20 mL dH_2O at 60°C; 25 mL 0.3 M cacodylate buffer with 4 mM $CaCl_2$ and 5 mL 25% glutaraldehyde were added.

All tissue samples were rinsed 5 times for 3 minutes in 150 mM sodium cacodylate and 2 mM $CaCl_2$ solution. Then the samples were immersed in freshly prepared 4% OsO_4 and 3% $K_4[Fe(CN)_6]$ in 0.3 M cacodylate buffer with 4 mM $CaCl_2$ at r.t. for 1 h – 5 minutes before the end of the hour, the samples were microwaved 3 times with 10-second-breaks in between intervals.

For the next step, 1% aqueous thiocarbohydrazide (TCH) solution had to be prepared: 0.1 g TCH in 10 mL ddH_2O was heated at 60°C for 1 h, gently shaken every 10 min and finally filtered with a 0.22 µm Millipore syringe filter. The tissue samples were then incubated in the TCH solution for 20 min at r.t. – after 9;13;15 min, all samples were microwaved.

All samples were rinsed 5 times for 3 minutes each in ddH_2O at r.t. and were then stored overnight (16 h) at 4°C. On the next day, the samples were incubated in 2% OsO_4 in ddH_2O solution for 30 min at r.t. - after 5;15;25 min, all samples were microwaved. Afterwards, the samples were rinsed 5 times for 3 minutes in ddH_2O at r.t.

The tissue samples were split into two times 3 groups (T43a/b/c and T46a/b/c) before further treatments – samples T43a/b/c were not exposed to microwaves any more during the rest of the preparation procedure. The Samples T43a/T46a were immersed in a 1% solution of uranyl acetate in ddH_2O; the samples T43b/T46b were immersed in a 1% solution of UAR-EMS ("Uranyl Acetate Replacement – Electron Microscopy Sciences" stain, a mixture of samarium and gadolinium triacetate; product number 22405) in ddH_2O; the samples T43c/T46c served as control group and were immersed in ddH_2O. All samples were stored at 4°C overnight (20 h).

The procedure was continued on the next day, by rinsing all samples 5 times for 3 minutes in ddH_2O at r.t., and then microwaving the T46-batch 3 times with 10-second-breaks in between

intervals. Afterwards, all samples were incubated in Walton's lead aspartate solution for 30 min at 60°C. Walton's lead aspartate solution was prepared by dissolving 0.066 g lead nitrate in 10 mL 0.03 M L-aspartic acid solution, and the solution's pH was adjusted to 5.5 with 1 M KOH. Then the samples were rinsed 5 times for 3 minutes in ddH_2O at r.t.

The next step was dehydration of the samples: they were incubated in 30;50;70;90;100% and a second time 100% EtOH for 2 times 8 minutes and microwaved after 0;1;8 minutes.

Following the dehydration series, all samples were infiltrated with 100% propylene oxide for 10 minutes at r.t. and microwaved; this step was repeated with fresh propylene oxide, but the samples were stored at 4°C overnight after being microwaved once for 1 minute. After that, the samples were infiltrated with 25% Hard-Plus 812 resin (EMS) in 100% propylene oxide for 2 h at r.t. and were microwaved three times for 1 minute; this step was repeated with 50% Hard-Plus 812 resin in 100% propylene oxide. Then infiltration was continued with 75% Hard-Plus 812 resin in 100% propylene oxide for 3 h at r.t. and microwaving three times for 1 minute. Afterwards, the samples were infiltrated with 100% Hard-Plus resin overnight at r.t. in a desiccator. The resin was exchanged, and infiltration was continued for another 3 h.

The preparation was completed by embedding the tissue samples in Hard-Plus 812 resins in flat moulds and polymerizing the resin at 60°C for two days.

Microwaving was performed in a cold bath at 80 W for 30 seconds (unless otherwise stated in the procedure).

3.1.2 Making Glass Knives for Trimming and Cutting

For the preparation of ultrathin sections and blocks for examination by TEM and SEM, the use of diamond and glass knives is required, the making of latter being described hereafter.

The glass knives are prepared from 6x25x400 mm glass strips employing the balanced break method as described by Hagler in [20]: A clean glass strip is balanced on the balance pins and held in place with the clamp. An equal breaking force is applied on both sides before the glass is scored with the diamond scribe. Within ca. 3 minutes, the fracture propagates through the glass strip, yielding two shorter glass strips of equal length. This procedure is repeated with the shorter glass strips until 16 square pieces (25x25 mm) are obtained (Figure 20 illustrates this process).

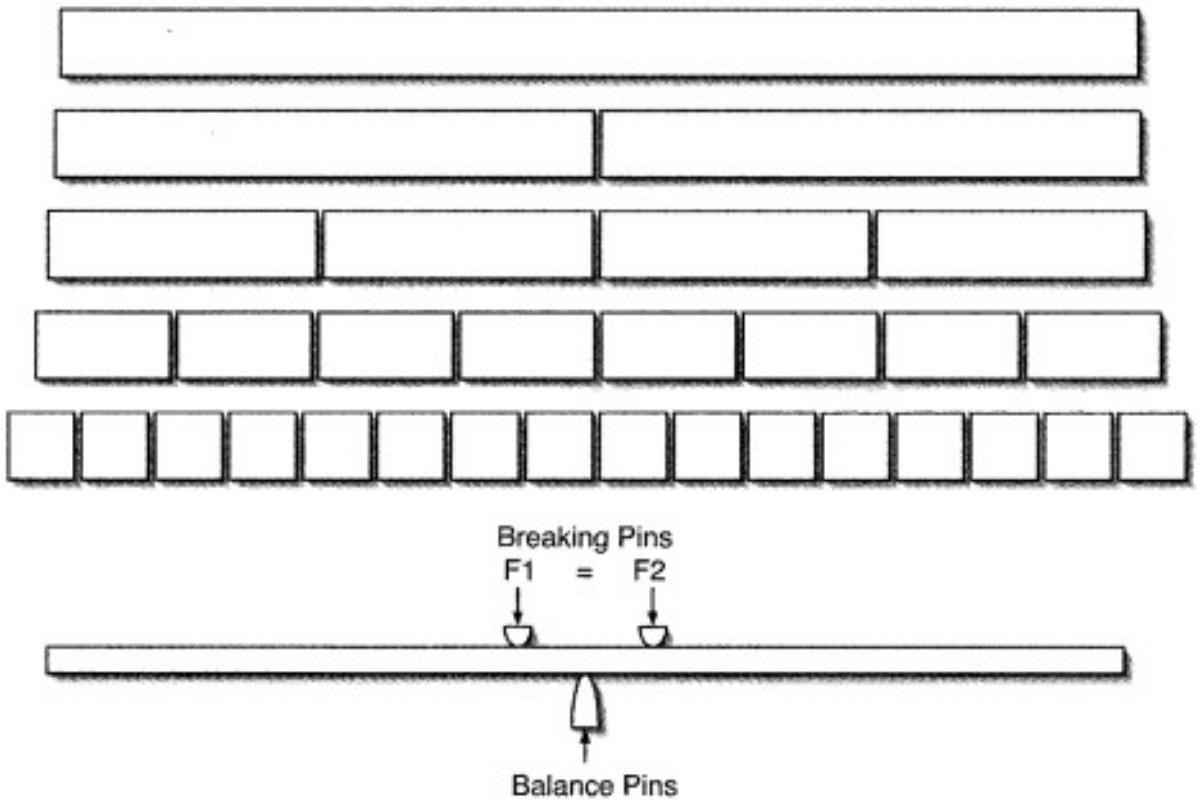

Figure 20: Preparing square pieces from a glass stripe; figure taken from [20]

Two glass knives can be obtained from one square glass piece by cutting the square piece from one edge to the opposite one (Figure 21). The scribe is set in a way that the obtained knife angle is approximately 48°, giving two knives and counterpieces from one square piece (Figure 22). The desired knife is supposed to have a small (<0.1 mm) and parallel counterpiece (Figure 23). Another criterion for the quality of glass knives is the Wallner line: Good knives are a result of slow breaks, which are indicated by a Wallner line that is parallel and close to the edge of the knife (Figure 23).

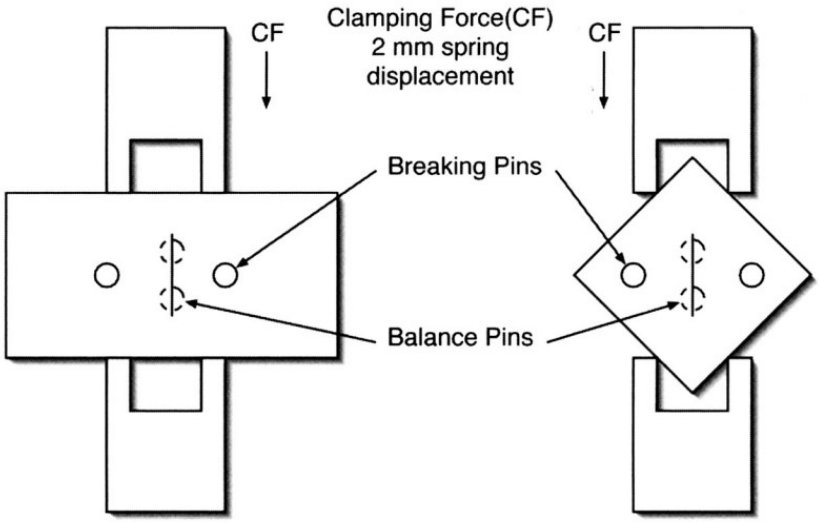

Figure 21: Top view on the process of preparing square pieces and glass knives; CF = clamping force; figure modified from [20]

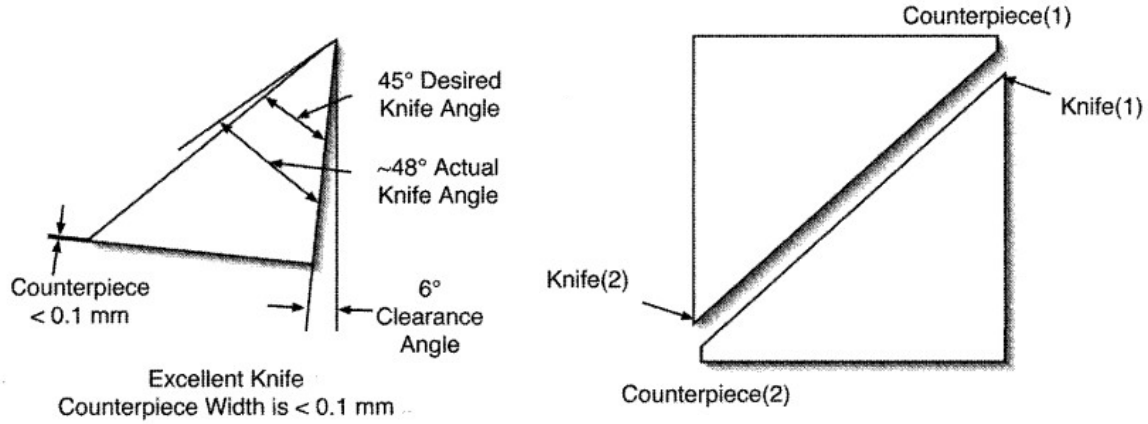

Figure 22: Left: Comparison of the desired and actual knife angle; Right: Illustration of the relationship between counterpiece and knife edge; figure modified from [20]

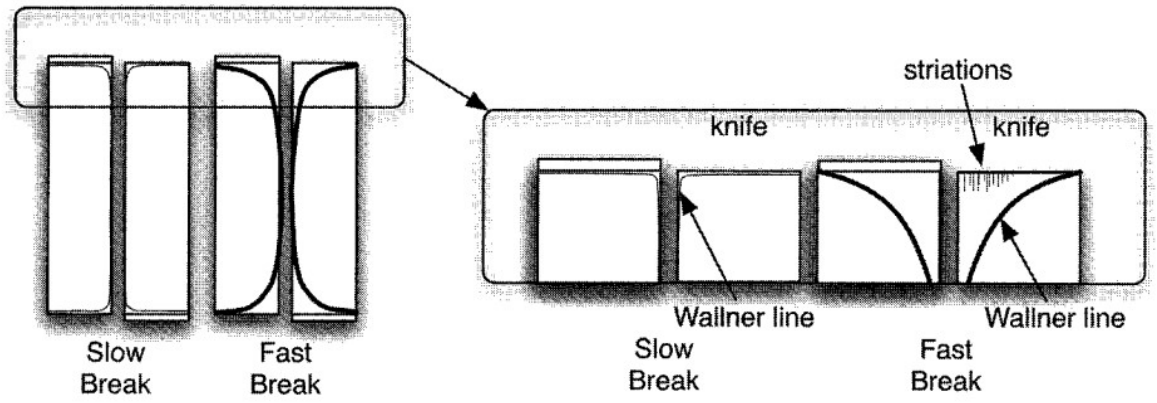

Figure 23: Comparison of Wallner lines for different breaking speeds: slow breaks give better knives and result in Wallner lines that are parallel and close to the knife's edge; figure taken from [20]

3.1.3 Ultramicrotomy – Trimming and Cutting

Thick sections, ultrathin sections and blocks for examination by light microscopy, TEM and SEM were prepared with a ultramicrotome, employing the previously prepared glass knives. The ultramicrotome makes it possible to expose the specimen and obtain thin sections from it by cutting off slice after slice from the resin block.

Before resorting to the ultramicrotome for precise cutting, the resin around the specimen is removed using a razor blade. The aim is to remove as much resin as possible without destroying the specimen, while at the same time the block is shaped into a square frustum (truncated pyramid), where the specimen lies below the top surface of the frustum. Subsequently, slices are removed from the top surface with the ultramicrotome until the (entirety of the) face cuts the specimen. At this point, thick sections (400 nm) can be obtained from the specimen for examination with a light microscope. In order to do this, a boat is used. The boat is filled with 10% acetone in H_2O and sections that are now cut with the knife will float on the water surface in the boat. The sections can then be transferred to a glass slide, dried by placing them on a heating block – staining for examination with a light microscope is then performed with 1% toluidine blue for 1 minute.

Ultrathin sections (~70 nm) for examination by TEM can be obtained similarly to thick sections: Instead of 10% acetone in H_2O, only H_2O is used. The actual thickness of the sections in the boat can be estimated based on the sections' colour and chloroform vapours can be used to stretch the sections [20]. The ultrathin sections are collected on a copper grid. For a preliminary examination, ultrathin sections (70 nm) were cut with a glass knife. For the sections used in the contrast measurement, a diamond knife was employed to cut sections with 40;70;90 nm thickness.

For (SBF-)SEM, a cube, which shall be completely filled by the sample, is cut from the frustum in the following way: The top surface is removed from the frustum until the cross-sectional area of the sample is large enough (in theory: ≥ 400x400 nm). Now, one slant of the frustum is removed – 400 nm are cut off. The specimen holder is then rotated by 90° and the next slant is removed. The last step is repeated two more times, exposing a cube with 400 nm edge length.

The obtained cube is mildly heated, cut off from the resin block and glued to a specimen holder (the cut face shall be glued to the specimen holder!). This large cube is then sputter coated with gold. Now an even smaller cube with an edge length of 200 nm is cut from the large cube with the ultramicrotome). The small cube is then sputter coated with gold.

3.1.4 Additional staining for preliminary sample examination by TEM

Several ultrathin sections (70 nm) for a preliminary sample examination of the cellular ultrastructure by TEM were stained additionally with ethanolic UAc and aqueous lead citrate solutions as follows:

The ethanolic UAc solution was prepared by dissolving 2.6 g UAc in 20 ml 50% EtOH in a brown bottle. The solution was mixed for two hours and filtered (0.45 µm pores) before use.

The lead citrate solution was prepared by dissolving 0.03 g lead citrate in 20 mL boiled (then cooled), deionized water and adding 0.2 mL 10 M NaOH.

In both cases, a droplet of the solution is placed on the clean surface of a piece of parafilm, and the grid with the ultrathin sections is placed on this droplet in such a way that the sections are in contact with the droplet. The staining is first performed with uranyl acetate in a metal box (protection against radiation; also, UAc is sensitive to light, it precipitates [21]). After incubation for 30 minutes, the grids are washed in 30% ethanol. Once the grids are dried, they are placed on droplets of the lead citrate solution in the same fashion as they were placed on the uranyl acetate solution droplets. The staining is performed in a covered Petri dish, in which a wetted NaOH pellet was placed (to avoid formation of lead carbonate). After incubation for 20 minutes the grids are washed in ddH_2O.

Prior to examination in TEM, the sections were coated with a carbon layer (JEE 4C, JEOL).

3.1.5 Preliminary sample examination by TEM

The previously stained ultrathin sections were examined by TEM in order to check, whether the primary sample preparation (chemical fixation and embedding in resin) were successful. One of the obtained micrographs is shown in figure 24, important structural features have been labelled exemplary.

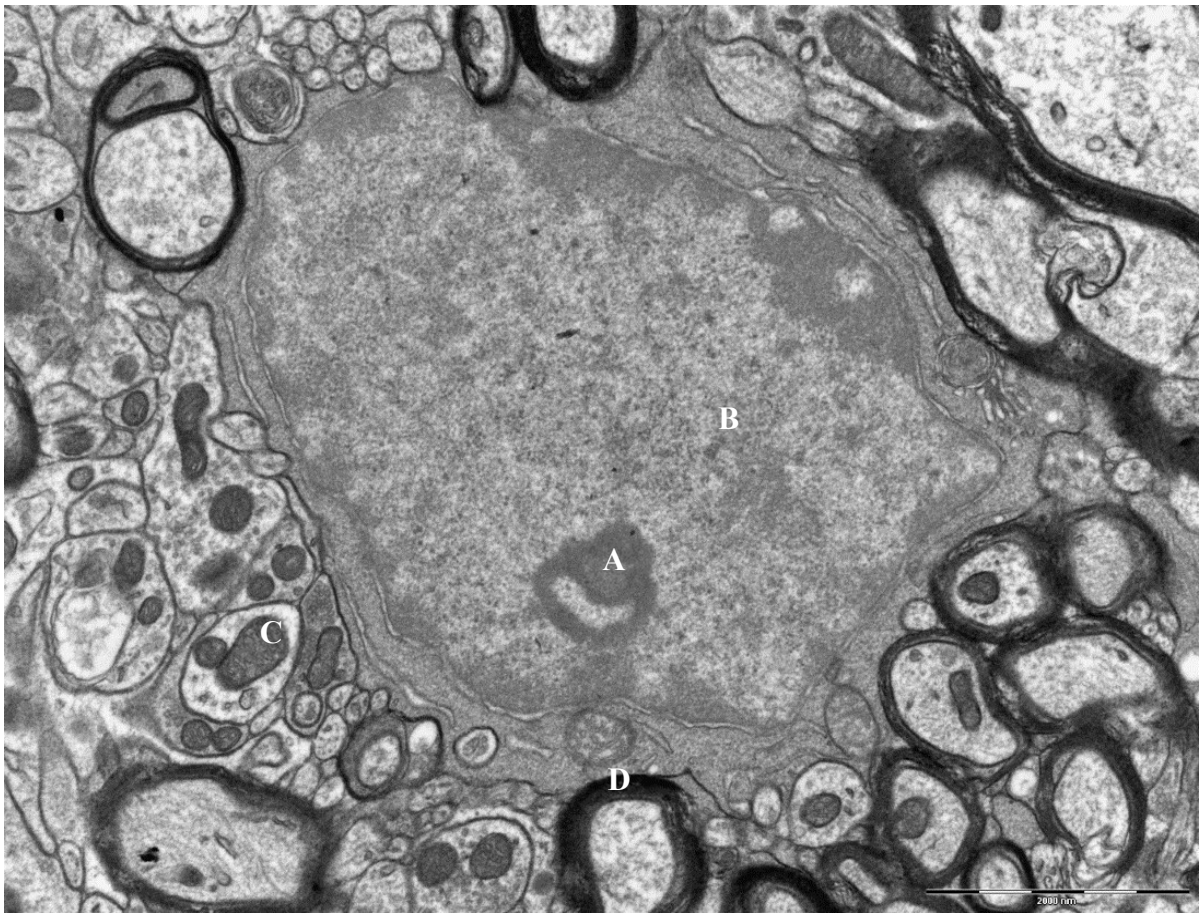

Figure 24: Electron micrograph of T46b (70 nm); the bar in the lower right corner corresponds to a length of 2 µm; *Labels*: A = nucleolus, B = nucleus, C = mitochondria; D = myelin sheath

3.1.6 Sample examination by SEM

As described in the ultramicrotomy section, cubes with 400 nm edge length were prepared from T46a, T46b and T46c (500 µm slice thickness, 100 mm/s). Each cube was then cut off with a scalpel and glued (cyanoacrylate) to an aluminium specimen stage. The connection between the block and the pin was covered in silver paint, to establish grounding of the block. After leaving the paint to dry overnight, cubes with 200 µm edge length were cut from the large cube and sputter coated with gold (3 min, Baltec SCD 050). After that, the surface of the block was cut off with a diamond knife.

The samples were then checked for charging by SEM (JEOL 7401F). The SEM micrographs were acquired at an accelerating voltage between 1-8 kV (BSE at 3 kV), a working distance of 8 mm, using probe current 7, emission 10 µA, a resolution of 1280x1024 px. The BSE images were captured using a retractable, below-lens, improved Autrata YAG detector. The SE images were recorded using either the upper in-lens detector for secondary electrons (SEI), or the lower, below-lens Everhart-Thornley detector (LEI).

3.1.7 Image Acquisition for contrast measurement by TEM

For the contrast measurement, micrographs of tissue and tissue-free resin (background) of seven groups were recorded: In order to investigate the influence of section thickness on the contrast, three groups were prepared from T46a (50, 70, 90 nm section thickness); in order to compare the contrast of different staining agents, two more groups of sections were prepared from T46b (70nm) and T46c (70 nm); in order to assess the influence of microwaving on the contrast, two more groups were prepared from T43a (70 nm) and T43c (70 nm).

Prior to examination in TEM, the sections were coated with a carbon layer.

The micrographs were recorded with TEM JEOL 2100, at 200 kV, 5000x magnification, 2672x2672 px resolution. The apertures and spot size (1) were not changed during the measurements, and the dose was checked to be at 2.00 e/Å^2 every ten minutes. 30 images of tissue and background were acquired each in the following way: A region containing tissue was searched and five (non-overlapping) images were taken of this region. For the next five images, a different ultrathin section on the grid was selected. After moving the camera, each image was taken after waiting for 60 seconds in order to reduce the drift. This process was repeated until 30 images had been acquired. The procedure was repeated with regions containing no tissue, in order to obtain the background images. Figure 25 below shows one example each of a region containing tissue or resin only.

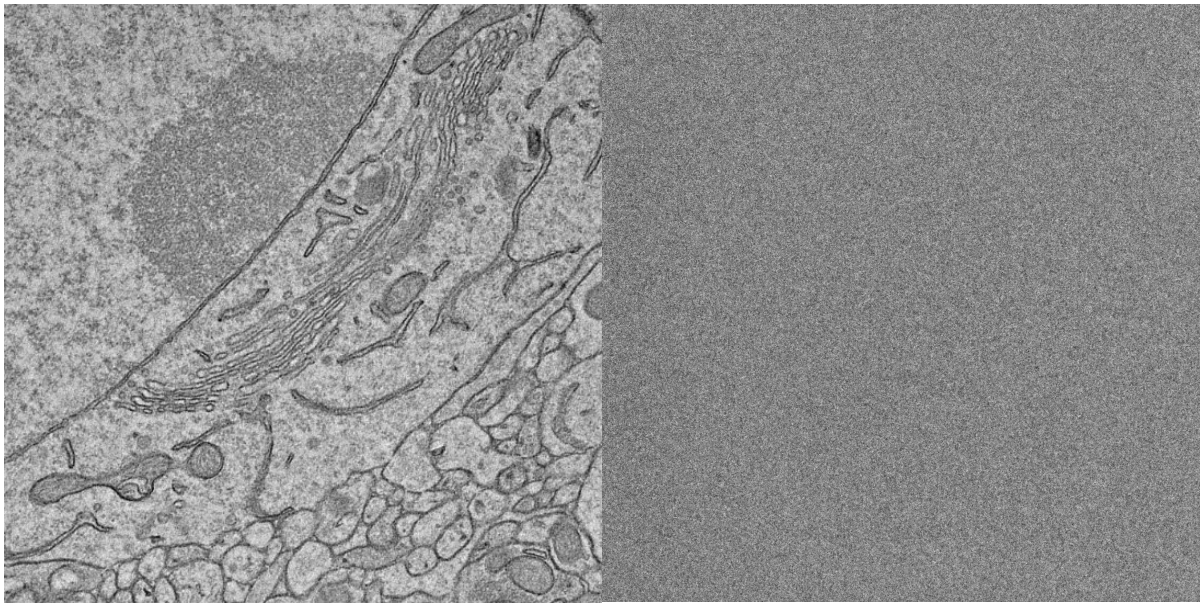

Figure 25: Electron micrographs of T46a (70 nm); *left*: tissue; *right*: resin

3.1.8 Contrast evaluation of membranes

The foundation for the contrast evaluation was measuring the grey values of the previously obtained micrographs (2672x2672 px, Bit depth 16). Only 10 out of the 30 images of each group were used for the manual measurement of the membrane contrast. For the other measurements all 30 images in each group were used. Using ImageJ, several measurements were performed:

Global Contrast:

The contrast was evaluated by measuring the minimum, maximum and mean grey value and the grey value's standard deviation of an entire image. The (Michelson) contrast was then calculated according to the formulas:

$$C_1 = \frac{GV_{Max} - GV_{Min}}{GV_{Max} + GV_{Min}}$$

$$C_2 = \frac{\left(\frac{GV_{Max} - GV_{Min}}{2}\right)}{\sigma}$$

Where:

C_1 … Michelson contrast

C_2 … contrast (SD)

GV_{Max} … maximum grey value

GV_{Min} … minimum grey value

σ … standard deviation

Automated Measurement of Membrane Contrast:

Employing ImageJ, separate masks for the foreground (membranes) and the background (the rest of the image) were created from the electron micrographs. The masking was done with Huang's threshold method.

The contrast was then evaluated by measuring the mean grey value of the membranes and the mean grey value of the background – a border region of 10 pixels around the membranes was omitted from the measurement of the background. The Michelson contrast was than calculated according to the formula above: Here GV_{Max} is the background's mean grey value and GV_{Min} is the membrane's mean grey value.

The masking and grey value measurement was automated with ImageJ, whereas the contrast calculation was carried out manually.

Manual Measurement of Membrane Contrast – Sigmoid Fit:

Another contrast measurement of the membranes was performed, but this time the grey values were measured manually with ImageJ. The procedure for measuring the grey values is exemplary visualized in figure 26: An image is opened in ImageJ and the contrast is adjusted (which has only a visual effect but does not alter the information in the image). After zooming in on a perpendicular membrane, a line (ca. 10 pixels long) is drawn from the middle of the membrane towards the background using the "straight"-tool. The grey values along this line are measured and visualized with the "Plot Profile" command (Analyze → Plot Profile; "Ctrl+K" on a Windows PC). Pressing the "Save" button below the plot saves the measured grey values as .xls-file.

The measured grey values were then fitted to a sigmoid curve using MATLAB (Figure 27). The minimum and maximum values of the fitted sigmoid curve were then used for the calculation of the Michelson contrast as described previously.

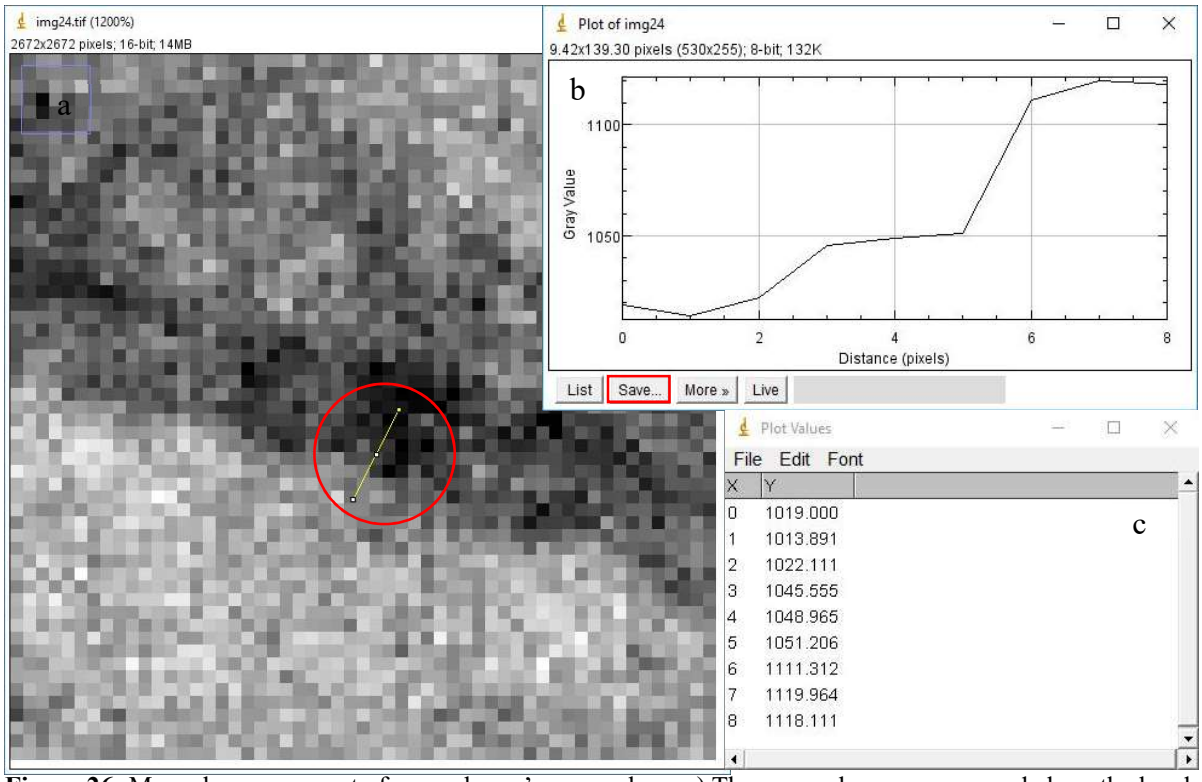

Figure 26: Manual measurement of a membrane's grey values: a) The grey values are measured along the hand-drawn, yellow line; b) the measured grey values can be plotted and then saved; c) measured grey values as displayed in ImageJ

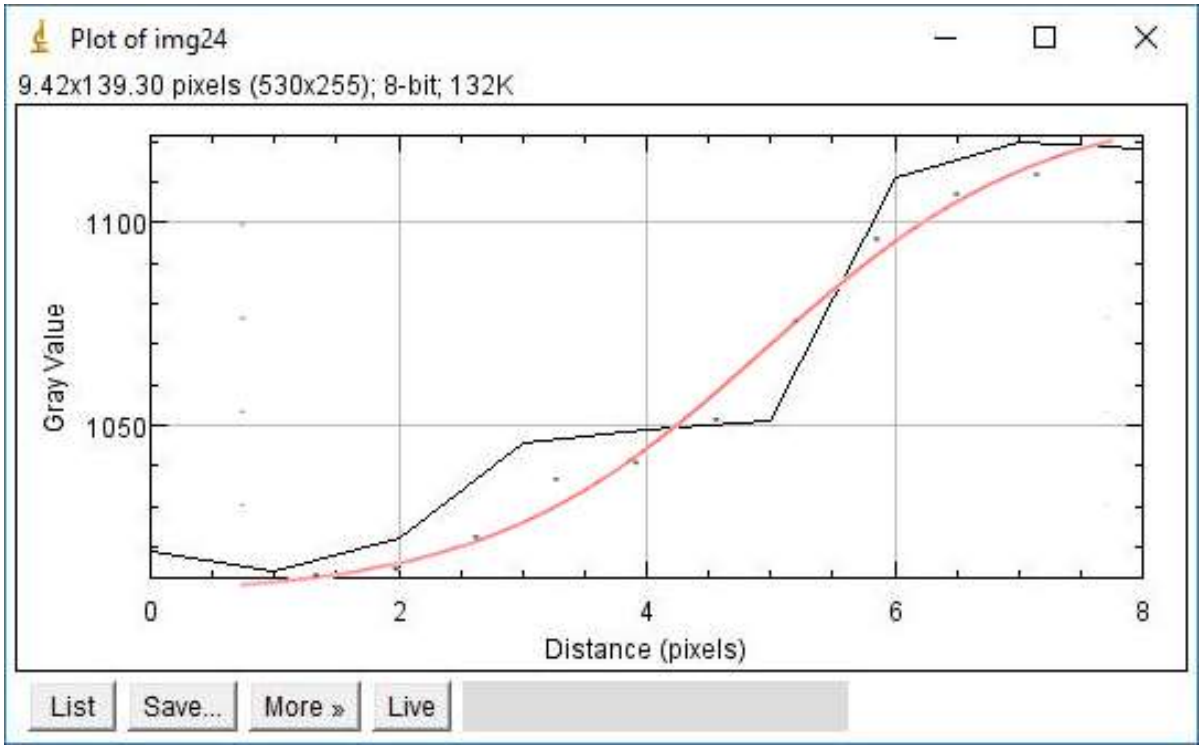

Figure 27: Illustration of a sigmoid fit; This image is not an accurate representation, but should give an idea of the process; (Composition)

Global Contrast Factor:

In addition to the Michelson contrast, also the Global Contrast Factor ("GCF") of the images was calculated. Back in 2005, the GCF was introduced as a new contrast measure, which is based on the local contrast at different resolutions. The concept of GCF is supposed to describe the contrast of human perception more accurately than previously used methods [22].

4. Publication bibliography

[1] Kremer, A.; Lippens, S.; Bartunkova, S.; Asselbergh, B.; Blanpain, C.; Fendrych, M. et al. (2015): Developing 3D SEM in a broad biological context. In *Journal of microscopy* 259 (2), pp. 80–96. DOI: 10.1111/jmi.12211.

[2] Transmission Electron Microscopy | Central Microscopy Research Facility (2018). Available online at https://cmrf.research.uiowa.edu/transmission-electron-microscopy, updated on 4/28/2018, checked on 4/28/2018.

[3] Scanning Electron Microscopy | Central Microscopy Research Facility (2018). Available online at https://cmrf.research.uiowa.edu/scanning-electron-microscopy, updated on 5/5/2018, checked on 5/5/2018.

[4] Kohl, Helmut; Reimer, Ludwig (2008): Transmission Electron Microscopy. Physics of Image Formation. New York, NY: Springer-Verlag New York (Springer Series in Optical Sciences, 36).

[5] Titze, Benjamin; Genoud, Christel (2016): Volume scanning electron microscopy for imaging biological ultrastructure. In *Biology of the cell* 108 (11), pp. 307–323. DOI: 10.1111/boc.201600024.

[6] Misell, D. L.; Burdett, I. D. J. (1977): Determination of the mass thickness of biological sections from electron micrographs. In *Journal of microscopy* 109 (2), pp. 171–182. DOI: 10.1111/j.1365-2818.1977.tb01127.x.

[7] Available online at https://nau.edu/cefns/labs/electron-microprobe/glg-510-class-notes/signals/, checked on 5/9/2018.

[8] Deerinck, T. J.; Shone, T. M.; Bushong, E. A.; Ramachandra, R.; Peltier, S. T.; Ellisman, M. H. (2018): High-performance serial block-face SEM of nonconductive biological samples enabled by focal gas injection-based charge compensation. In *Journal of microscopy* 270 (2), pp. 142–149. DOI: 10.1111/jmi.12667.

[9] Kuo, John (Ed.) (2014): Electron Microscopy. Methods and Protocols. 3rd ed. 2014. Totowa, NJ: Humana Press (SpringerLink Bücher, 1117).

[10] Hoffman, Elizabeth A.; Frey, Brian L.; Smith, Lloyd M.; Auble, David T. (2015): Formaldehyde crosslinking: a tool for the study of chromatin complexes. In *The Journal of biological chemistry* 290 (44), pp. 26404–26411. DOI: 10.1074/jbc.R115.651679.

[11] Kawahara, Jun-ichi; Ishikawa, Keiichiro; Uchimaru, Tadafumi; Takaya, Haruo (1997): Polymer Modification. Boston, MA: Springer.

[12] Hua, Yunfeng; Laserstein, Philip; Helmstaedter, Moritz (2015): Large-volume en-bloc staining for electron microscopy-based connectomics. In *Nature communications* 6, p. 7923. DOI: 10.1038/ncomms8923.

[13] Tapia, Juan Carlos; Kasthuri, Narayanan; Hayworth, Kenneth J.; Schalek, Richard; Lichtman, Jeff W.; Smith, Stephen J.; Buchanan, JoAnn (2012): High-contrast en bloc staining of neuronal tissue for field emission scanning electron microscopy. In *Nature protocols* 7 (2), pp. 193–206. DOI: 10.1038/nprot.2011.439.

[14] Wangensteen, Douglas; Bachofen, Hans; Weibel, Ewald R. (1981): Effects of glutaraldehyde or osmium tetroxide fixation on the osmotic properties of lung cells. In

Journal of microscopy 124 (2), pp. 189–196. DOI: 10.1111/j.1365-2818.1981.tb00313.x.

[15] Hosogi, Naoki; Nishioka, Hideo; Nakakoshi, Masamichi (2015): Evaluation of lanthanide salts as alternative stains to uranyl acetate. In *Microscopy (Oxford, England)* 64 (6), pp. 429–435. DOI: 10.1093/jmicro/dfv054.

[16] Zechmann, B.; Zellnig, G. (2009): Microwave-assisted rapid plant sample preparation for transmission electron microscopy. In *Journal of microscopy* 233 (2), pp. 258–268. DOI: 10.1111/j.1365-2818.2009.03116.x.

[17] Nguyen, Huy Bang; Thai, Truc Quynh; Saitoh, Sei; Wu, Bao; Saitoh, Yurika; Shimo, Satoshi et al. (2016): Conductive resins improve charging and resolution of acquired images in electron microscopic volume imaging. In *Scientific reports* 6, p. 23721. DOI: 10.1038/srep23721.

[18] Odriozola, Adolfo; Llodrá, Jaime; Radecke, Julika; Ruegsegger, Céline; Tschanz, Stefan; Saxena, Smita et al. (2017): High contrast staining for serial block face scanning electron microscopy without uranyl acetate.

[19] Amako, Kazunobu; Takade, Akemi; Umeda, Akiko; Yoshida, Masaru (1993): Imaging of the Surface Structures of Epon Thin Sections Created with a Glass Knife and a Diamond Knife by the Atomic Force Microscope. In *Journal of Electron Microscopy*. DOI: 10.1093/oxfordjournals.jmicro.a051012.

[20] Hagler, Herbert K. (2007): Ultramicrotomy for biological electron microscopy. Chapter 5. In *Methods in molecular biology (Clifton, N.J.)* 369, pp. 67–96. DOI: 10.1007/978-1-59745-294-6_5.

[21] EM Sample Preparation Contrasting. Available online at https://www.leica-microsystems.com/fileadmin/academy/2013/Contrasting_final.pdf, checked on 4/22/2018.

[22] Matković, Krešimir; Neumann, László; Neumann, Attila; Psik, Thomas; Purgathofer, Werner (2005): Global Contrast Factor - a New Approach to Image Contrast. DOI: 10.2312/COMPAESTH/COMPAESTH05/159-167.

5. Abbreviations

Table 3: Used Abbreviations

Abbreviation	Meaning
ATUM-SEM	Automated Tape-collecting Ultramicrotome Scanning Electron Microscopy/e
BSE	backscattered electron(s)
$CaCl_2$	calcium chloride
ddH2O	double distilled water
dH2O	distilled water
EM	Electron Microscopy
EtOH	ethanol
FIB-SEM	Focused Ion Beam Scanning Electron Microscopy/e
GdAc	gadolinium triacetate
$K_4[Fe(CN)_6]$	potassium ferrocyanide
LM	light microscope
OsO_4	osmium tetroxide
PbAsp	lead aspartate
r.t.	room temperature
SBF-SEM	Serial Block-Face Scanning Electron Microscopy/e
SEM	Scanning Electron Microscopy/e
SmAc	samarium triacetate
ssTEM	serical section Transmission Electron Microscopy
TCH	thiocarbohydrazide
TEM	Transmission Electron Microscopy/e
UAc	uranyl acetate

6. Appendices

Appendix I

Table 4: Results of the calculation for the global contrasts C_1 and C_2; SD = standard deviation

name	T43a 70 nm	T43c 70 nm	T46a 50 nm	T46a 70 nm	T46a 90 nm	T46b 70 nm	T46c 70 nm
C_1	12.64	13.14	11.06	14.67	11.77	10.62	11.16
SD C_1	1.53	1.74	1.22	2.98	2.18	0.83	1.06
C_2	4.85	5.60	5.08	5.37	5.18	5.10	5.22
SD	26.96	24.34	23.64	27.84	23.22	22.01	22.45
SD C_2	0.26	0.54	0.35	0.36	0.34	0.25	0.51

Table 5: Results of the calculation of contrast after automated preselection of membranes by ImageJ

name	T43a 70 nm	T43c 70 nm	T46a 50 nm	T46a 70 nm	T46a 90 nm	T46b 70 nm	T46c 70 nm
C_1	1.9538	1.6699	1.6272	1.5498	1.6494	1.4449	1.5471
SD C_1	0.3255	0.2378	0.2567	0.5769	0.4544	0.2481	0.1882

Table 6: Results of the calculation of contrast from manually measured grey values of the membranes

name	T43a 70 nm	T43c 70 nm	T46a 50 nm	T46a 70 nm	T46a 90 nm	T46b 70 nm	T46c 70 nm
C_1	0.062	0.057	0.061	0.070	0.063	0.050	0.050
SD	0.018	0.016	0.012	0.017	0.014	0.015	0.015

Table 7: Results of the calculation of the Global Contrast Factors

name	T43a 70 nm	T43c 70 nm	T46a 50 nm	T46a 70 nm	T46a 90 nm	T46b 70 nm	T46c 70 nm
GCF	2.95	2.75	2.63	3.03	2.57	2.67	2.56
SD	0.26	0.16	0.17	0.49	0.22	0.13	0.13